chemosensors

MDPI

Review

Metal Oxide Semiconductor Nanostructure Gas Sensors with Different Morphologies

Ali Mirzaei [1], Hamid Reza Ansari [2], Mehrdad Shahbaz [3], Jin-Young Kim [4], Hyoun Woo Kim [5,6] and Sang Sub Kim [4,*]

1 Department of Materials Science and Engineering, Shiraz University of Technology, Shiraz 71557-13876, Iran; mirzaei@sutech.ac.ir
2 Department of Electrical and Electronics Engineering, Shiraz University of Technology, Shiraz 71557-13876, Iran; hr.ansari@sutech.ac.ir
3 Department of Materials Science and Engineering, Urmia University, Urmia 5766-151818, Iran; m.shahbaz@urmia.ac.ir
4 Department of Materials Science and Engineering, Inha University, Incheon 22212, Korea; piadote@naver.com
5 Division of Materials Science and Engineering, Hanyang University, Seoul 04763, Korea; hyounwoo@hanyang.ac.kr
6 The Research Institute of Industrial Science, Hanyang University, Seoul 04763, Korea
* Correspondence: sangsub@inha.ac.kr

Abstract: There is an increasing need for the development of low-cost and highly sensitive gas sensors for environmental, commercial, and industrial applications in various areas, such as hazardous gas monitoring, safety, and emission control in combustion processes. Considering this, resistive-based gas sensors using metal oxide semiconductors (MOSs) have gained special attention owing to their high sensing performance, high stability, and low cost of synthesis and fabrication. The relatively low final costs of these gas sensors allow their commercialization; consequently, they are widely used and available at low prices. This review focuses on the important MOSs with different morphologies, including quantum dots, nanowires, nanofibers, nanotubes, hierarchical nanostructures, and other structures for the fabrication of resistive gas sensors.

Keywords: semiconductor; metal oxide; morphology; gas sensor; sensing mechanism

Citation: Mirzaei, A.; Ansari, H.R.; Shahbaz, M.; Kim, J.-Y.; Kim, H.W.; Kim, S.S. Metal Oxide Semiconductor Nanostructure Gas Sensors with Different Morphologies. *Chemosensors* **2022**, *10*, 289. https://doi.org/10.3390/chemosensors10070289

Academic Editors: Joana Rodrigues and Nuno Santos

Received: 8 June 2022
Accepted: 18 July 2022
Published: 21 July 2022

1. Introduction

Although industrial modernization facilitates social, cultural, and economic development globally, it results in the consumption of enormous amounts of energy every day. Consequently, the toxic gas and vapor emissions released into the atmosphere cause air pollution, which has been identified as a major concern in most countries. Air pollution adversely affects humans, animals, vegetation, and materials [1]. Air pollution is mainly caused by the presence of NO_2, SO_2, CO, and O_3 gases, along with volatile organic compounds (VOCs), lead, and particulate matter ($PM_{2.5}$ and PM_{10}) in the air [2–4]. Air pollution, owing to its fluidity and diffusion, has a more adverse impact on human behavior and economic growth than soil and river pollution [4]. About 12% of deaths in 2019 were related to air pollution. In addition, it has been reported that air pollution was responsible for approximately 20% of deaths from cardiovascular diseases [5]. Globally, air pollution is the fourth-highest cause of mortality [6]. For example, the World Health Organization (WHO) reports that approximately 200,000 people die every year from air pollution in Bangladesh [7]. According to a WHO report, 92% of the global population lives in cities with air pollution exceeding the WHO limits, indicating the need for further monitoring and control of air pollutant gases and vapors [8].

Toxic gases are harmful to human bodies whether at low (chronic exposure) or high (acute exposure) concentrations. The threshold limit value (TLV) is reported as the maximum concentration of gas exposure permitted for 8 h without serious health effects. The

TLVs for CO, H_2S, and NO_2 are 50, 10, and 3 ppm, respectively, indicating the high toxicity of these gases [9]. Thus, the development of sensitive sensors for detecting these toxic gases is vital.

The human olfactory system is very sensitive and complex, and comprises several million olfactory receptor cells that contain nearly 900 olfactory receptor genes (Figure 1). Thus, it can almost instantaneously detect even extremely low concentrations of odorant molecules. It can detect 1 in 2.5 billion parts of the air containing ethyl mercaptan, usually added as an odorant to natural gas [10].

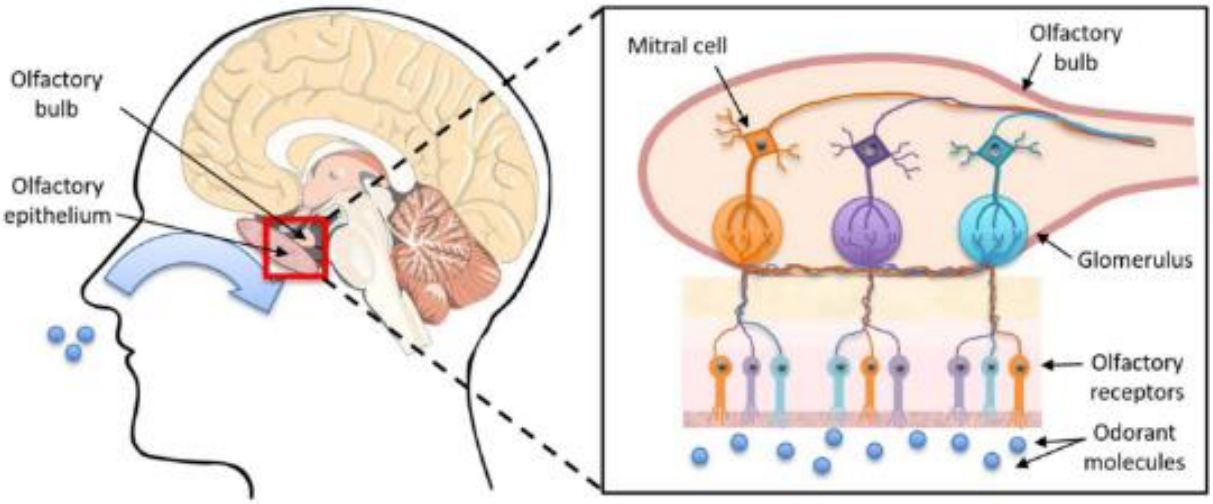

Figure 1. Schematic of the human olfactory system. Reprinted with permission from Ref. [11]. Copyright 2018, MDPI.

However, some toxic gases—such as CO—lack odor. Moreover, some gases at very low concentrations cannot be detected by the human olfactory system. To precisely detect dangerous gases and vapors, sensitive and high-performance gas sensors with the ability to detect low amounts of gases with a fast response are necessary. Furthermore, such sensors should be highly stable and cost-effective. Considering this, gas sensors using different sensing materials and working principles have been introduced. Even though chromatography techniques can be used for the detection of gases, the equipment is heavy, expensive, and needs a skilled operator. Thus, gas sensors are the preferred devices for gas-sensing applications.

Among all gas sensors, resistive-based gas sensors comprising metal oxide semiconductors (MOSs) meet almost all criteria for a good gas sensor, although their selectivity and sensing temperatures need to be optimized. MOS sensors are very popular and widely used in different areas to detect up to 150 different types of gases and vapors, including oxidizing and reducing gases [12]. Bardeen and Brattain were the first scientists to report gas-sensitive effects on germanium in 1952 [13]. Two years later, in 1954, Heiland noted that the change in the partial pressure of oxygen is influenced by the semiconducting properties of ZnO [14]. After one decade, in 1962, Seiyama et al. [15] reported the first gas sensor based on ZnO, in which the adsorption and desorption of gases changed its conductivity. In 1967, Shaver used Pt and other noble metals as dopants in WO_3 for the first time [16]. Several years later, Taguchi used SnO_2 as the first commercial sensor [17]. Since then, many gas sensors using different materials with various morphologies have been reported.

Different MOSs can be employed to produce gas sensors. However, a large band gap (E_g) along with a low activation energy of the centers is suitable for use in MOS-based gas sensors. Generally, for room-temperature gas sensors, a low-band gas is advantageous [18]. Other properties of a good MOS are high stability as well as the high mobility of the charge carriers [19].

Figure 2 schematically indicates a schematic of a gas-sensing device [20]. MOS-based gas sensors are generally deposited as thick or thin films on insulating substrates (flat or tubular), such as SiO_2 or Al_2O_3, equipped with interdigitated electrodes (e.g., Au, Pt, and Ag/Pd) to read out the sensor resistance. Electrodes can be deposited on the substrate before and after depositing the sensing film. This provides significant flexibility in the fabrication process because of the compatibility with the sensing material. Generally, interdigitated electrodes are used to read the sensor resistance, and their length and gap size can affect the gas response. An excellent discussion on the influence of the electrode parameters on the gas response can be found in the study by Korotcenkov [21]. In addition, an integrated heater or external heater is employed to enable the sensor temperature to reach the final value. Generally, the sensing temperature of MOS-based gas sensors is high, and it is often necessary to heat the sensor to the required temperatures.

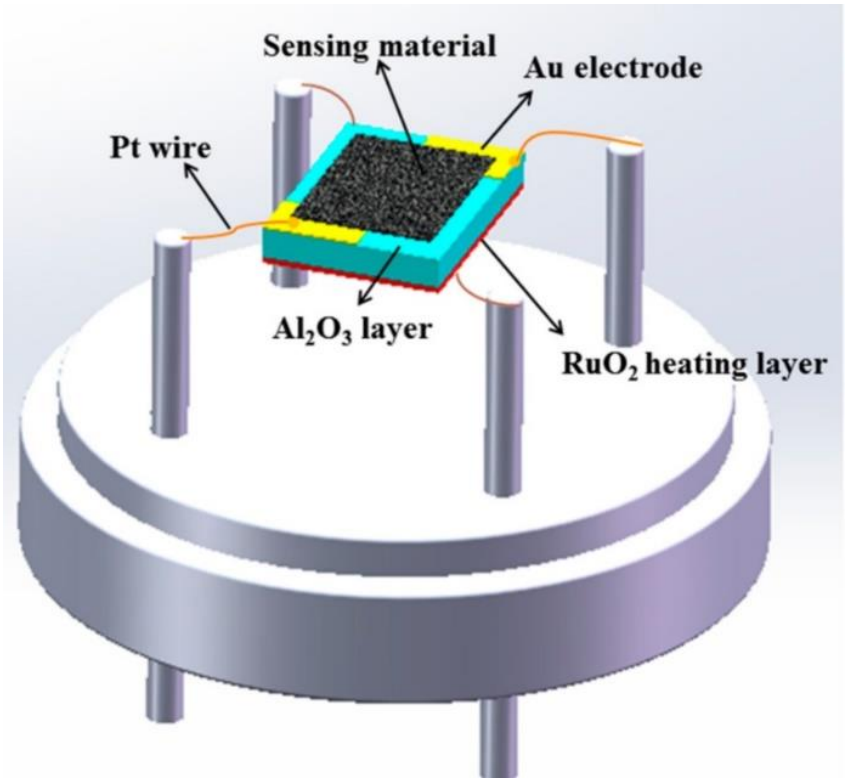

Figure 2. Schematic illustration of an MOS-based gas sensor, showing the sensing material, electrodes, and heater. Reprinted with permission from Ref. [20]. Copyright 2020, MDPI.

Gas-sensing measurement systems are categorized into two types: dynamic and static. In both cases, the system requires gas valves and gas flow controllers to inject the target gas into the chamber. In addition, a system for controlling the sensing temperature is required, and the output signal is continuously recorded using a computer. In a dynamic system, the desired gas concentrations are continuously introduced to the gas chamber through tubes, and the resistance of the sensor in an air target gas atmosphere at various temperatures is registered. In a static system, the target gas is introduced into the chamber and evaporated upon contact with the heater. The exact size of the gas chamber should be defined. Upon stabilization of the sensor resistance, the gas chamber door or outlet is opened, and fresh air is introduced into the chamber [9].

To date, different MOSs have been used for sensing studies. They are either n-type or p-type MOSs. In most cases, the n-type MOS is preferred, because most of the n-type MOSs are thermally stable and can function at low oxygen partial pressures. Furthermore, the resistance of n-type oxides decreases upon exposure to reducing gases, contributing to facile compatibility with the measurement systems [18]. According to Kim et al. [22], SnO_2

is the most popular MOS for gas-sensing applications, and ZnO is the second-most-used MOS for sensing studies.

It is well accepted that the variation of the resistance in the presence of the target gas is the basic mechanism of gas detection by resistive gas sensors. A schematic of the sensing mechanism for n- and p-type MOS sensors in the presence of an oxidizing gas is shown in Figure 3. Because of the high electronegativity of oxygen and the extraction of electrons by oxygen species on the surface of the gas sensor, an electron depletion layer is formed on the surface of n-type gas sensors, and a hole accumulation layer is formed on the surface of p-type gas sensors, as shown in Figure 3a,c, respectively. When an n-type sensor is exposed to an oxidizing gas, electrons are further extracted, leading to an increase in the width of the electron depletion layer and an increase in the sensor resistance (Figure 3b). In a reducing gas atmosphere, the width of the electron depletion layer decreases, resulting in a decrease in the sensor resistance. Upon exposing p-type MOS gas sensors to an oxidizing gas, more electrons are extracted, resulting in the expansion of the hole accumulation layer and a decrease in the sensor resistance (Figure 3d). For reducing gases, the inverse is true, and the resistance increases.

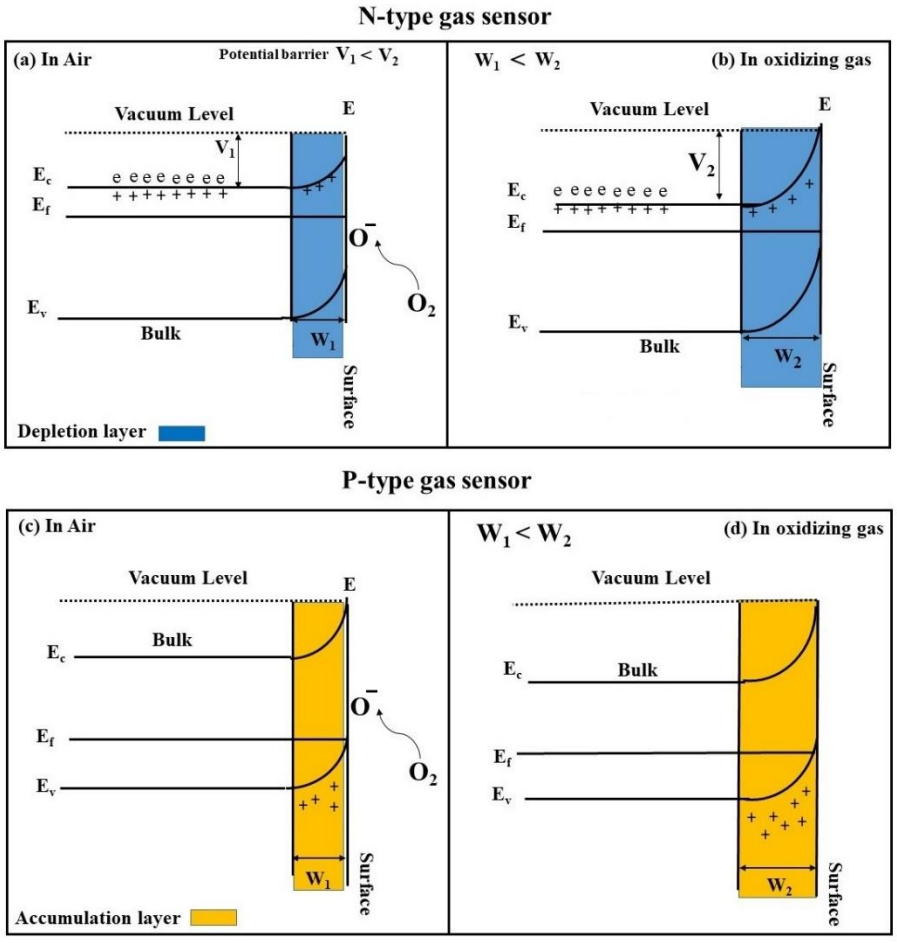

Figure 3. The general gas-sensing mechanism of (**a**,**b**) n-type and (**c**,**d**) p-type MOS gas sensors in the presence of air and an oxidizing gas.

In resistive-based gas sensors, morphology plays a vital role in the response of the gas sensor. As gas molecules are adsorbed on the surface of the sensing layer, the resistance changes, and this modulation of the resistance contributes to the appearance of a sensing signal. Accordingly, a higher surface area provides more adsorption sites for incoming gas molecules, leading to the enhancement of the gas response. In recent years, many attempts have been made to develop sensing materials with a high surface area, such as nanowires

and nanofibers. This review mainly focuses on the most widely used morphologies and structures for gas-sensing applications. In the following sections, the main features of MOS-based gas sensors are discussed in detail.

2. MOS-Based Gas Sensors with Different Morphologies

2.1. Quantum-Dot-Based Gas Sensors Using MOSs

Morphology engineering is an important approach for enhancing the gas-sensing features of MOS-based gas sensors, and MOS materials with different morphologies have been explored for gas-sensing purposes. The main goal of using novel morphologies for sensing studies is to increase the surface area. The larger the surface area, the greater the availability of adsorption sites, resulting in the adsorption of more gas molecules on the surface of the gas sensor, along with the appearance of a higher sensing signal. For sensing studies, zero-, one-, two-, and three-dimensional morphologies have been explored. Quantum dots (QDs) are zero-dimensional (0D) semiconductor nanoparticles, where the motion of charge carriers is confined in all three directions. Thus, the energy difference between energy bands changes depending on the size of the particle, and it is possible to tune the band gap of QDs by changing their size. Accordingly, the electrical properties of QDs can be engineered by controlling the dot size [23]. Owing to the extremely small size of QDs, when the QDs are exposed to air, they are depleted of electrons, and subsequent exposure to the target gas leads to extensive modulation of the electrical resistance, leading to a high sensing signal. In addition, owing to their large resistance variation and good electrical properties, most QD-based gas sensors can work at low temperatures. In [24], different approaches to synthesized SnO_2 QDs are reviewed. Recently, QDs have been widely used for sensing studies [25,26]. For example, Zhu et al. [27] used SnO_2 QDs with a size of 5–10 nm for ethanol sensing at 200 °C at a fixed relative humidity (RH) of 40%. The sensor exhibited a response to 220–300 ppm of ethanol gas. For SnO_2 with a size larger than the space-charge layer, EDLs form on the surface of NPs, and upon exposure to a reducing gas, the modulation of resistance occurs, as shown in Figure 4a. However, for SnO_2 QDs with a size smaller than the space-charge layer, the QDs become depleted from electrons in the air. In this case, a flat band is formed, and the energetic difference between the conduction band and the Fermi level increases (Figure 4b). In the presence of ethanol, the electrons are released back into the SnO_2 QDs. At this point, the QDs become more conductive, resulting in a significant increase in the sensor conductivity.

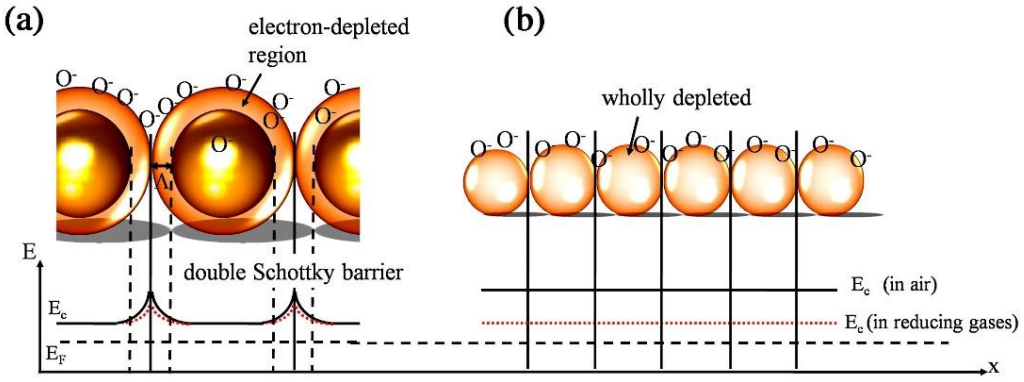

Figure 4. The sensing mechanism of SnO_2 NPs and SnO_2 QDs. (**a**) when the particle size is larger than space-charge layer of SnO_2 (**b**) When the particle size is smaller than space-charge layer of SnO_2. Reprinted with permission from Ref. [27]. Copyright 2016, Elsevier.

2.2. Nanowire-Based Nanomaterial Gas Sensors

Among different morphologies, nanowires (NWs) with aspect ratios greater than 20 [28] are highly popular for sensing applications, owing to their high surface area, straightforward preparation methods, ease of gas sensor fabrication, high and rapid response to the target gas, long-term stability, and high crystallinity [29,30]. Accordingly, several studies

have realized the enhanced gas-sensing capacity of NW-based gas sensors [31,32]. In [33], various methods to synthesize NWs are discussed in detail.

Among different MOSs with NW morphology, SnO_2 NWs are very popular for sensing purposes [34–37]. SnO_2 has a band gap of 3–4 eV, depending on the synthesis method, size, surface states, and impurities [38]. However, most studies have reported a band gap of 3.7 eV for this MOS [39]. SnO_2 is the most stable n-type oxide, and is extensively used in the preparation of semiconductor gas sensors. Its high electron mobility (~160 $cm^2/V{\cdot}s$) makes it a key choice for sensing applications [19,40]. In addition, SnO_2 NWs exhibit good optical transparency and conductivity [41]. Wang et al. [42] performed one of the first studies on SnO_2 NWs for the detection of H_2 gas, and compared the results with those of SnO_2 nanorods (NRs). It was reported that owing to the higher surface area of NWs, size effects when the diameter of the NWs was less than the Debye length of SnO_2, and the small electrode gap of the SnO_2 NW gas sensor, a larger response was observed for the SnO_2 NWs at 300 °C than that for SnO_2 NRs. Notably, not only SnO_2 NWs, but also other MOS NWs, have been employed as gas sensors [43,44]. The construction of n–n and p–n junctions is a commonly employed strategy for improving the sensitivity of NW-based gas sensors [45]. Owing to the generation of these heterojunctions, the resistance of gas sensors is higher than that of the pure sensing material, and the subsequent modulation of resistance in the presence of target gases generates a high sensing signal for heterojunction gas sensors [46].

Branched NWs (e.g., nanoforests or nanotrees) are a special type of NWs that have recently been used for sensing applications. Their 3D morphology and numerous homo- or heterojunctions make the branching NWs highly popular for sensing studies. With high surface area, branched NWs can detect extremely low amounts of gases. Branched NWs also offer an increased number of carrier paths and improved conduction between the NW branches and backbones [47–49]. Several studies have elaborated on the enhanced gas-sensing properties of branched NWs [50,51]. Woo et al. [52] reported the p-xylene-sensing characteristics of Ni-doped branched ZnO NWs. As an n-type MOS, ZnO has high physical and chemical stability, a high electron mobility of up to 1000 cm^2/V, and a wide band gap—all of which are extremely favorable for sensing applications [53]. At 400 °C, it showed a high response to 42.44–5 ppm of p-xylene. The enhanced p-xylene gas response was related to the increased resistance modulation owing to the presence of numerous Schottky barriers between the branches. Importantly, selectivity was found to be related to the catalytic activity of Ni. Thus, by the combination of the high surface area of MOS and the catalytic effect of metals, it is possible to achieve highly sensitive gas sensors for practical applications. In another report, Bi_2O_3-branched SnO_2 NWs with a large surface area were prepared for NO_2-sensing studies [54]. Figure 5a–d show the relevant XRD and SEM characterizations, which demonstrate the formation of Bi_2O_3-branched SnO_2 NWs with the expected phase and morphology. The sensor exhibited a high response of 56.92 in the presence of only 2 ppm of NO_2 gas at 250 °C; this response is very high relative to that shown by other MOS-based gas sensors. This superiority was attributed to the presence of the following resistance modulation sources: (i) resistance modulation of the exposed surfaces of SnO_2 NWs, (ii) resistance modulation of the exposed surfaces of Bi_2O_3 NWs, (iii) resistance changes in the SnO_2–SnO_2 and Bi_2O_3–Bi_2O_3 homojunctions, and (iv) resistance modulation in the SnO_2–Bi_2O_3 heterojunctions. However, the contribution of SnO_2–Bi_2O_3 heterojunctions was the highest.

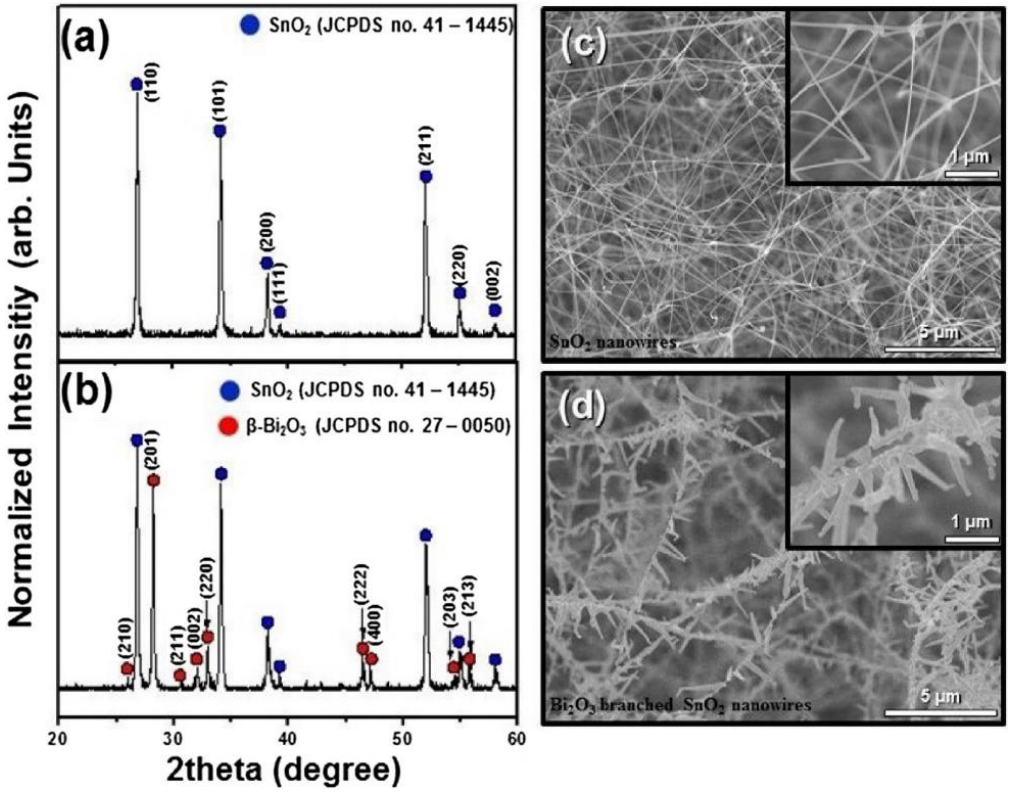

Figure 5. XRD spectra of (**a**) SnO_2 NWs and (**b**) Bi_2O_3-branched SnO_2 NWs. SEM images of (**c**) SnO_2 NWs and (**d**) Bi_2O_3-branched SnO_2 NWs. Reprinted with permission from Ref. [54]. Copyright 2018, Elsevier.

Overall, the high surface area along with numerous resistance modulation sources between the stem and branches of the NWs makes them suitable for gas-sensing studies. Furthermore, careful engineering of the branched NWs allows the fabrication of highly sensitive gas sensors based on MOS materials.

In addition to NWs and branched NWs, single NWs have recently been used for sensing various gases [55–57]. For instance, Tonezzer et al. [58] reported the use of a single SnO_2 NW for gas-sensing applications. By applying a thermal gradient to the single SnO_2 NW gas sensor and combining its responses at five various working temperatures from 200 to 400 °C, the sensor was able to distinguish seven different gases—namely, acetone, NH_3, CO, ethanol, H_2, NO_2, and toluene—and measure their concentrations. Even though it is possible to achieve single NW gas sensors with the present technology, it should be noted that the growth and realization of a single NW are difficult relative to other highly dense NWs. Moreover, because of the lack of heterojunctions, resistance modulation is relatively limited, and a high response cannot be expected from a single NW.

Core–shell (C–S) NWs are another category of NWs, where the core is coated with another metal oxide to form the C–S NWs [59]. In C–S nanostructures, the core and shell materials should be semiconductors. A good way to synthesize C–S NWs is by synthesizing the core NWs and then coating them with a shell using atomic layer deposition (ALD). In this way, the shell thickness can be easily adjusted by controlling the ALD cycles [60]. Thus, ALD is one of the most accurate techniques to control the shell thickness. The shell permits the diffusion of the gas into deeper parts of the sensor; accordingly, porous shells are more suitable for such applications. In C–S systems, the heterointerfaces are maximized, and heterojunctions are formed between the core and shell layers, resulting in superior modulation of the resistance [61]. Several C–S NW systems can be found in the literature for sensing studies [62–65]. However, it should be noted that there is an optimal shell thickness, at which the maximum response is obtained. This shell thickness is often close to the Debye length of the shell material [65]. The effect of shell thickness on

C–S systems has been extensively discussed in a review paper [66]. In addition, the use of noble metals as decoration on the surface of the shell layer is a widely used technique to enhance the sensitivity and selectivity of gas sensors to a particular gas. For example, Au functionalization on the surface of SnO_2–ZnO C–S NWs led to the enhancement of the sensing response to CO gas, as shown in Figure 6a,b [67]. The senor showed a high response of 26.6 to only 100 ppb of CO gas at 300 °C.

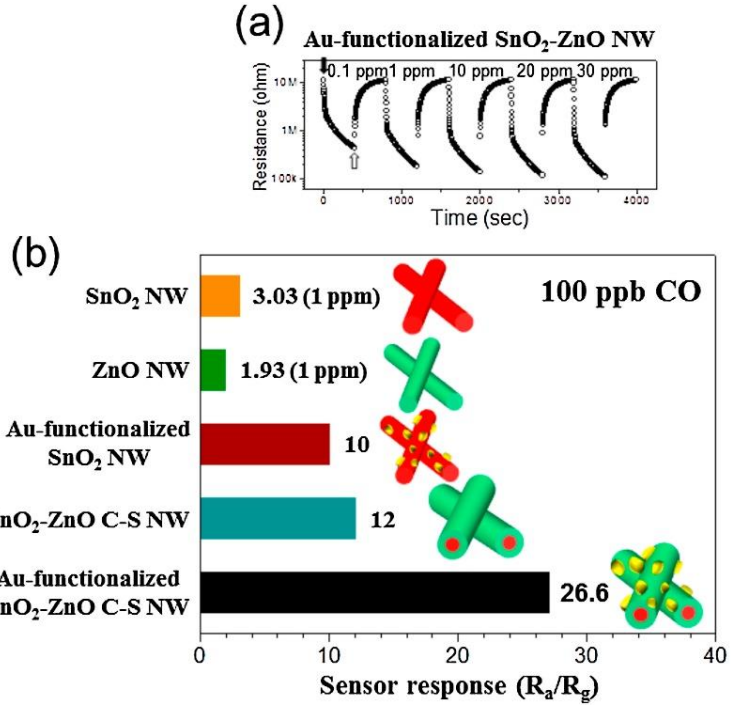

Figure 6. (**a**) Dynamic resistance curve of a Au-functionalized SnO_2–ZnO C–S NW gas sensor to low concentrations of CO gas. (**b**) Comparison between the responses of different gas sensors to 100 ppb of CO gas. Reprinted with permission from Ref. [67]. Copyright 2017, Elsevier.

In addition to the formation of SnO_2–ZnO heterojunctions, the formation of Au–ZnO Schottky barriers can contribute to the sensing signal (Figure 7a,b). The presence of Au changes the EDL thickness inside the ZnO shell, and in the presence of CO gas, variations in EDL width can enhance the sensing response (Figure 7c). Finally, Au with a catalytic (chemical sensitization) effect toward CO gas can promote the oxidation of CO gas on the surface of the gas sensor, leading to an enhanced response to CO gas (Figure 7d).

Careful design and engineering of the shell choice as well as of the shell thickness enables the formation of an additional EDL near the C–S interfaces, owing to electron trapping at the interfaces. Thus, the depletion of the entire shell layer from the charge carriers can occur. Furthermore, the large variations in the resistance of the C–S NWs can result in the generation of a high response. Moreover, potential barriers are formed, and the modulation of their height can contribute to the sensing signal [68]. In conclusion, C–S NW sensors are among the most promising novel nanostructures for gas-sensing studies. When the shell thickness is close to the Debye length of the shell material, they exhibit the highest gas-sensing performance. Additionally, a core with a larger or lower work function can significantly affect the optimized shell thickness.

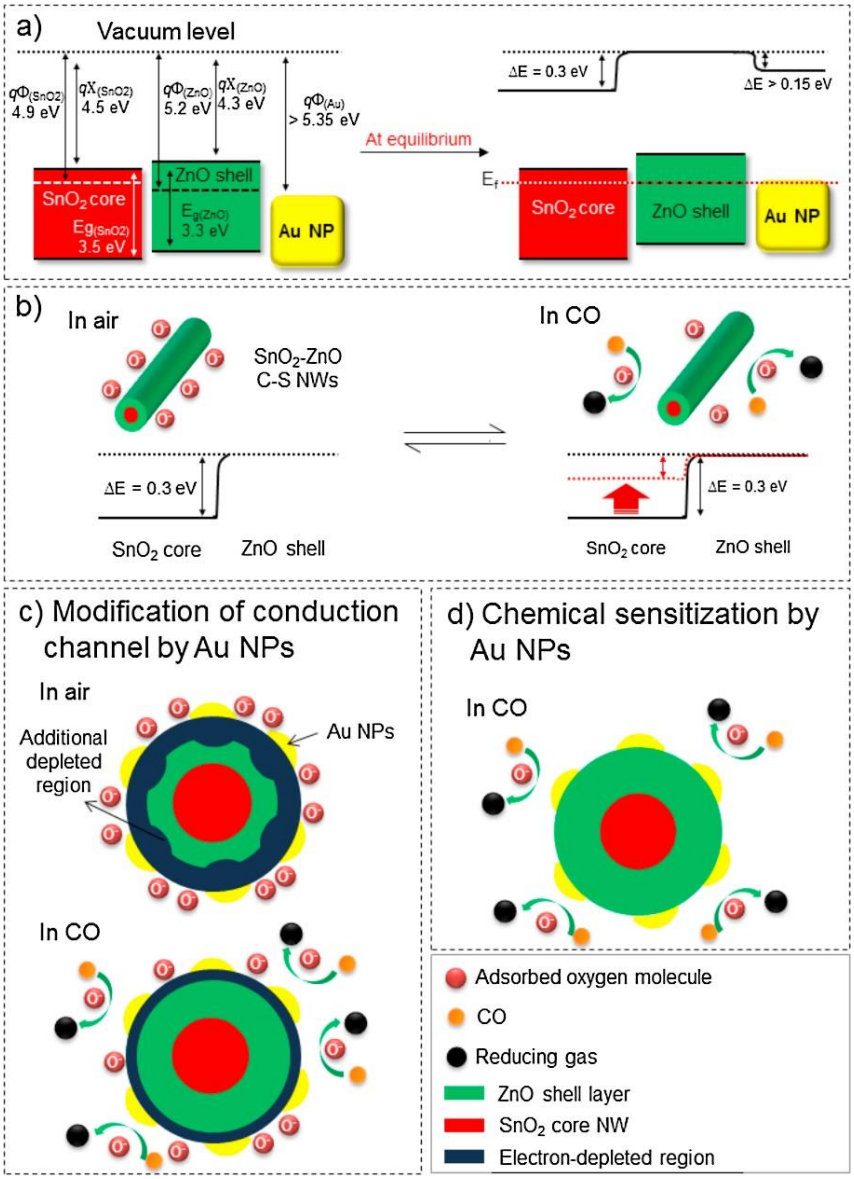

Figure 7. (**a**) Energy levels of SnO_2–ZnO and Au in vacuum and air after contact. (**b**) Modulation of SnO_2–ZnO heterojunctions in the presence of CO gas. (**c**) Modification of an EDL inside ZnO by Au. (**d**) Chemical sensitization of Au. Reprinted with permission from Ref. [67]. Copyright 2017, Elsevier.

Self-heated gas sensors are a new generation of MOS gas sensors in which an external voltage is applied to the electrodes of the gas sensors, leading to the generation of heat through the Joule heating mechanism inside the sensing material [69]. Notably, the operation of the gas sensor in this mode allows for extremely low power consumption, without the need for external heaters [69].

Typically, thin-film gas sensors with external heaters consume approximately 1–5 W of power, and MEMS-based sensors consume less than 30–50 mW of power. However, for a self-heated gas sensor, significantly lesser power (in the range of microwatts) is consumed [70]. Among the different morphologies, NWs are the most efficient for the development of self-heated gas sensors.

One NW in the self-heating mode can generate power densities 10,000 times higher than a heater [60]. The length of the NWs directly affects the heat generated inside the gas sensor, thus allowing Joule heating to warm the NWs and ensure a higher response to the target gas. Moreover, power is consumed at the microwatt scale due to the minimal thermal capacitance of the NWs [71]. Several studies have reported self-heating gas sensors

based on NWs [72–75]. For instance, Kim et al. [76] reported that CuO-decorated SnO_2–ZnO C–S NWs with an optimized shell thickness of 80 nm exhibited a good response to approximately 2–10 ppm of H_2S gas at a voltage as low as 5 V. This was attributed to the self-heating effect of the gas sensor, electrical contacts between the thick NWs, SnO_2–ZnO interfaces, and the presence of CuO. Kim et al. [77] fabricated a self-heated gas sensor based on Pd-decorated SnO_2–ZnO C–S NWs. The corresponding gas-sensing results are shown in Figure 8. A good response to 1.75–50 ppm of C_6H_6 gas was reported for the sensor, with a low applied voltage of 10 V and a low power consumption of 22.6 μW, which was related to the presence of heterojunctions as well as the catalytic effect of Pd.

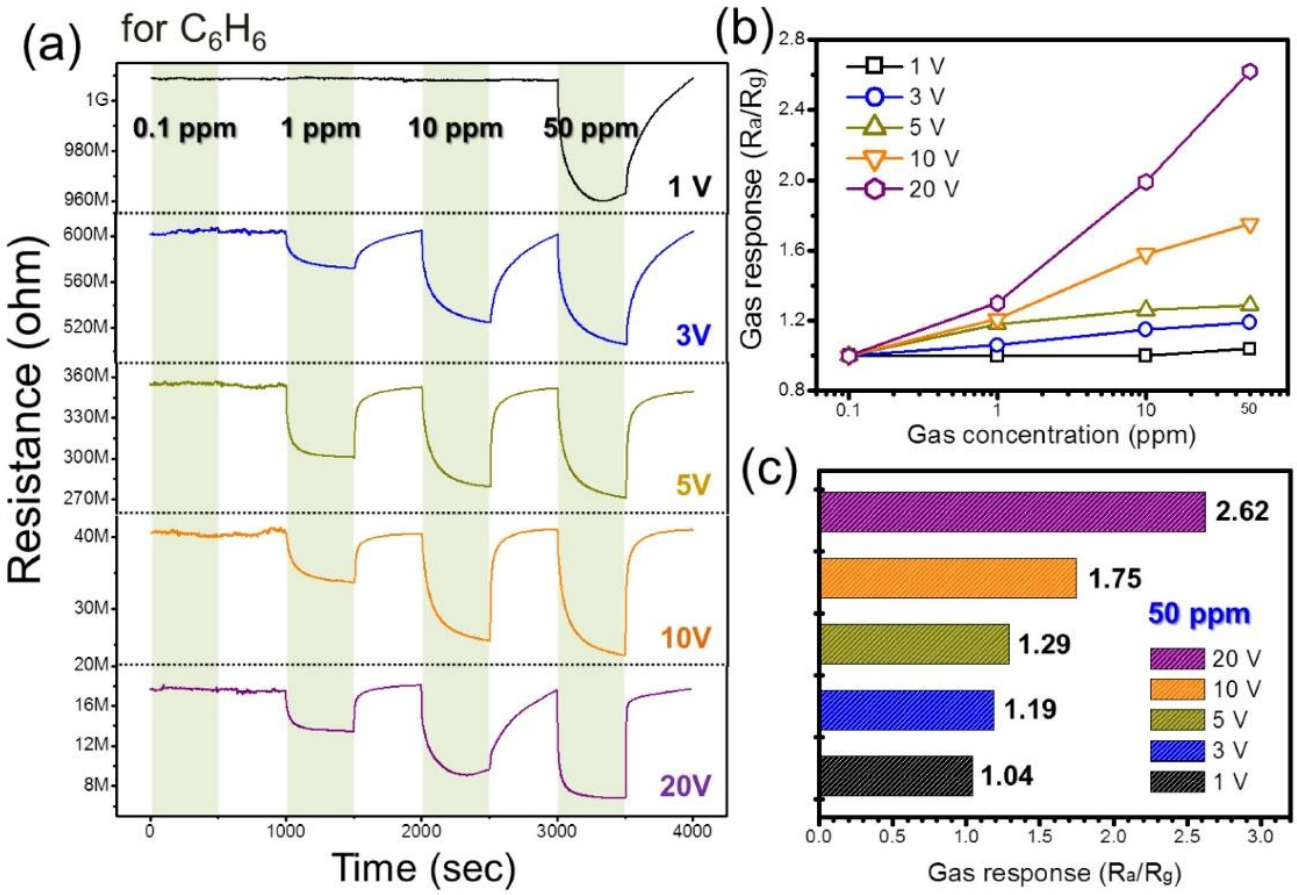

Figure 8. (**a**) Dynamic resistance curves of a Pd-functionalized SnO_2–ZnO C–S NW sensor at different values of applied voltages, and 0.1–50 ppm C_6H_6, at room temperature. (**b**) Corresponding calibration curves at different applied voltages. (**c**) Comparison between responses to 50 ppm C_6H_6 at different applied voltages. Reprinted with permission from Ref. [77]. Copyright 2020, Elsevier.

Although a self-heated single NW gas sensor has not yet been reported, a single NW gas sensor can consume very low power if the sensor works in self-heating mode. Since there is only one NW, it can be heated very fast with extremely low power consumption. Self-heated gas sensors with extremely low power consumption can be integrated in portable smart devices such as smart mobile phones.

2.3. Nanofiber-Based MOS Gas Sensors

Nanofibers (NFs) are another type of 1D material used in MOS gas sensors. Similar to NWs, NFs have an aspect ratio of more than 20. However, their surfaces have many nanograins, which result in a further increase in the surface area [78]. There are various methods to synthesize NFs; however, NFs are commonly produced using the electrospinning (ES) technique. The ES technique consists of a spinneret section, a high-voltage power supply, and a metal collector [79]. During electrospinning, NFs are formed from a liquid jet and subsequently elongated under a high voltage. The NF formation process consists of the following: (i) onset of jetting and development of a rectilinear jet, (ii) bending deformation along with solvent evaporation to form solidified NFs, and (iii) NF collection [80]. In a simplified view, a sol is initially prepared in this technique, and is subsequently poured into a syringe. Upon applying a high voltage to the sol with a defined viscosity, it is possible to collect extremely fine and long NFs on the collector placed at a fixed distance from the syringe. After calcination of the synthesized NFs at an appropriate temperature for sufficient time, the final diameter decreases due to evaporation of the solvent and organic materials [79].

By optimization of the ES technique parameters—such as the applied voltage, distance between the needle tip and the collector, flow rate, and temperature—it is possible to tune the diameter of the resulting NFs [81,82]. In particular, the viscosity of the solution can significantly affect the formation of long NFs [83]. If the viscosity of the ES solution is not adjusted to the desired value, NFs with beads are formed [83].

Furthermore, with a special type of ES technique, known as coaxial ES, it is possible to directly synthesize C–S NFs [84,85]. Many MOSs have been successfully synthesized using the ES technique for gas-sensing studies [86]. Similar to C–S NWs, the thickness of the shell layer should be adjusted to obtain the maximum response to the target gas. For example, Kim et al. [87] reported that in SnO_2–Cu_2O C–S NF gas sensors with different shell thicknesses, the sensor with a shell thickness of 30 nm gave the highest response to CO gas—it showed a response to 5–10 ppm of CO gas at 300 °C.

MOS-based gas sensors with NF morphology possess a high surface area, which provides many adsorption sites for the incoming gas molecules. Moreover, the nanograins on the surface of the NFs act as a powerful source of resistance modulation (Figure 9) [88].

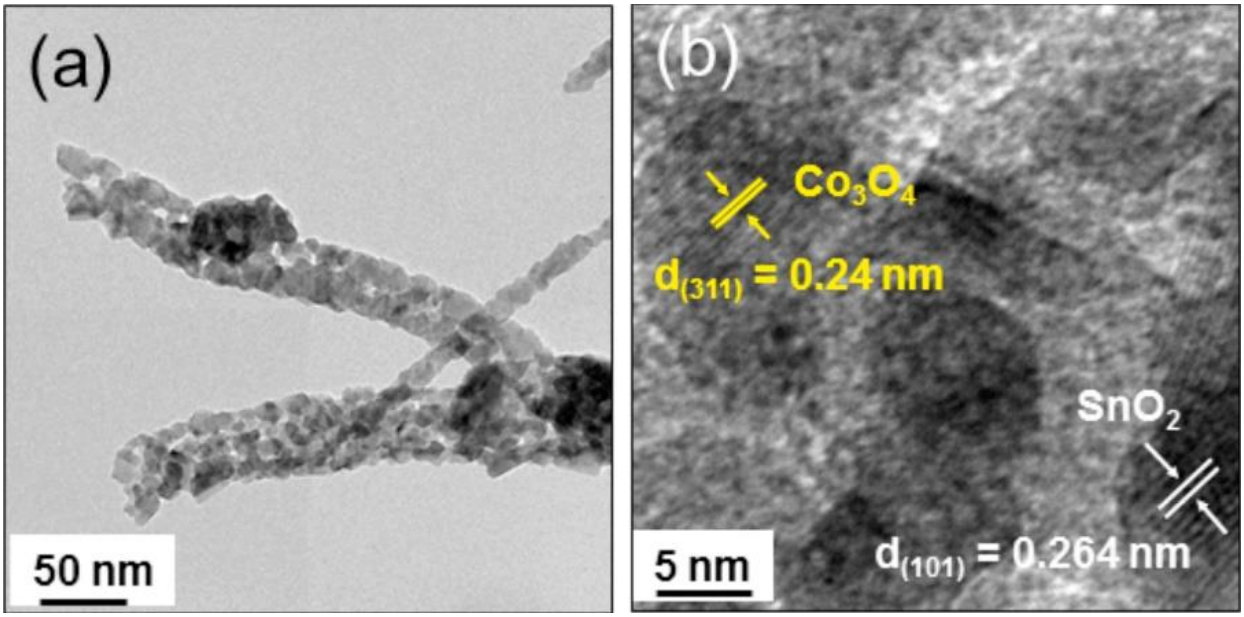

Figure 9. (**a**,**b**) TEM images of 0.5 SnO_2–0.5 Co_3O_4 composite NFs. Reprinted with permission from Ref. [88]. Copyright 2017, Elsevier.

To date, several types of NFs have been used for sensing applications. Pristine NFs [89], composite NFs [90], and noble-metal-decorated NFs [91] have been used for sensing studies. Other relevant morphologies include hollow NFs [92] and C–S NFs [93]. Hollow NFs, in particular, can provide a larger surface area for target gas molecules; hence, they are among the most popular types of NFs for sensing studies. A detailed discussion of the sensing mechanism of NFs can be found in the study by Kim et al. [94].

2.4. Nanotube-Based MOS Gas Sensors

Metal oxide nanotubes (NTs) have been studied less compared to their NW and NF counterparts [95]. This may be due to the difficulty in the synthesis of MOS NTs. Various techniques can be used for synthesizing MOS NTs. However, the most common method is the use of a hard or soft sacrificial template. Hard templates have been prepared using silica, carbon, and polystyrene beads, while soft templates have been fabricated from bubbles, polymer vesicles, emulsion droplets, and surfactant micelles. The core can be removed by dissolving in a solvent or calcination to generate hollow structures [96]. The main features of gas sensors based on hollow structures such as NTs are (i) wall permeability, (ii) wall thickness, and (iii) wall chemistry [97]. Although thinner NTs are expected to provide greater surface area and more adsorption sites for gas molecules [98], the presence of defects can sometimes alter the sensing properties. Hazra et al. investigated the effects of shell thickness on the sensing characteristics of TiO_2 NTs. Interestingly, the sensor with the thinnest wall and largest surface area did not show the highest response to the target gas, due to the lower amount of oxygen vacancies. The device with a thicker wall and sufficient oxygen vacancies exhibited the highest response [99]. In conclusion, MOS-based NTs for gas-sensing studies offer a high surface area owing to the hollowness of their structure, which can provide many adsorption sites for gas molecules.

2.5. Nanorod-Based MOS Gas Sensors

Nanorod-based gas sensors are another popular category of MOS materials for gas-sensing studies, owing to their unique electrical properties and high surface area provided by the NR morphology. The hydrothermal method provides a convenient, fast, versatile, and low-cost route for constructing well-ordered nanorod arrays [100–103]. However, other methods—such as chemical bath deposition (CBD), which is economical, straightforward, and scalable—can also be used to prepare NRs from different materials [104]. Chemical vapor deposition [105,106], metal–organic chemical vapor deposition [107,108], and pulsed laser deposition [109] are other methods for obtaining NRs in MOSs. NR-based MOS materials are popular for sensing studies because of their ease of production, high surface area, and compositional versatility.

2.6. Nanosheet-Based MOS Gas Sensors

Two-dimensional MOS nanostructured materials with a sheet-like morphology are popular for gas-sensing studies due to their high surface area. Only a few 2D MOS (MoO_3, WO_3, and SnO_2) analogs of graphene are known. Two-dimensional (2D) layered MOSs have strong in-plane bonds and weak van der Waals forces between layers, and gas molecules can be adsorbed on these sites. Thus, 2D layered MOSs can be employed for the production of gas sensors [110]. Apart from the naturally 2D layered MOSs, other MOSs can also be synthesized in a nanosheet-like morphology. For instance, Choi et al. [111] synthesized porous ZnO nanosheets using a solvothermal technique for NO_2 detection. The sensor exhibited a high response to 74.68–10 ppm of NO_2 gas at 200 °C. The width of the EDL increased in the presence of NO_2 gas, contributing to the sensing signal. Moreover, homojunctions were formed, and changes in the height of the homojunctions led to resistance modulation in the presence of NO_2 gas. Furthermore, the highly porous morphology and high specific surface area (11.51 m^2/g) contributed to the increased availability of active sites for NO_2 gas molecules [111].

In another study, Kim et al. [112] synthesized self-heated 2D pristine and Au-functionalized WS_2–SnO_2 core–shell NSs with different shell thicknesses of up to 60 nm on polyamide substrates. Bare and Au-decorated gas sensors with shell thicknesses of 15 and 30 nm exhibited the highest CO-sensing performance at a low voltage of 3.4 V. Figure 10a shows dynamic resistance curves of Au-decorated WS_2–SnO_2 with different shell thicknesses to 10 ppm CO at a fixed applied voltage of 3.4 V. Figure 10b shows the corresponding plots of response and resistance versus the shell thickness. The sensor with a shell thickness of 10 nm showed a high response to 12–10 ppm of CO gas.

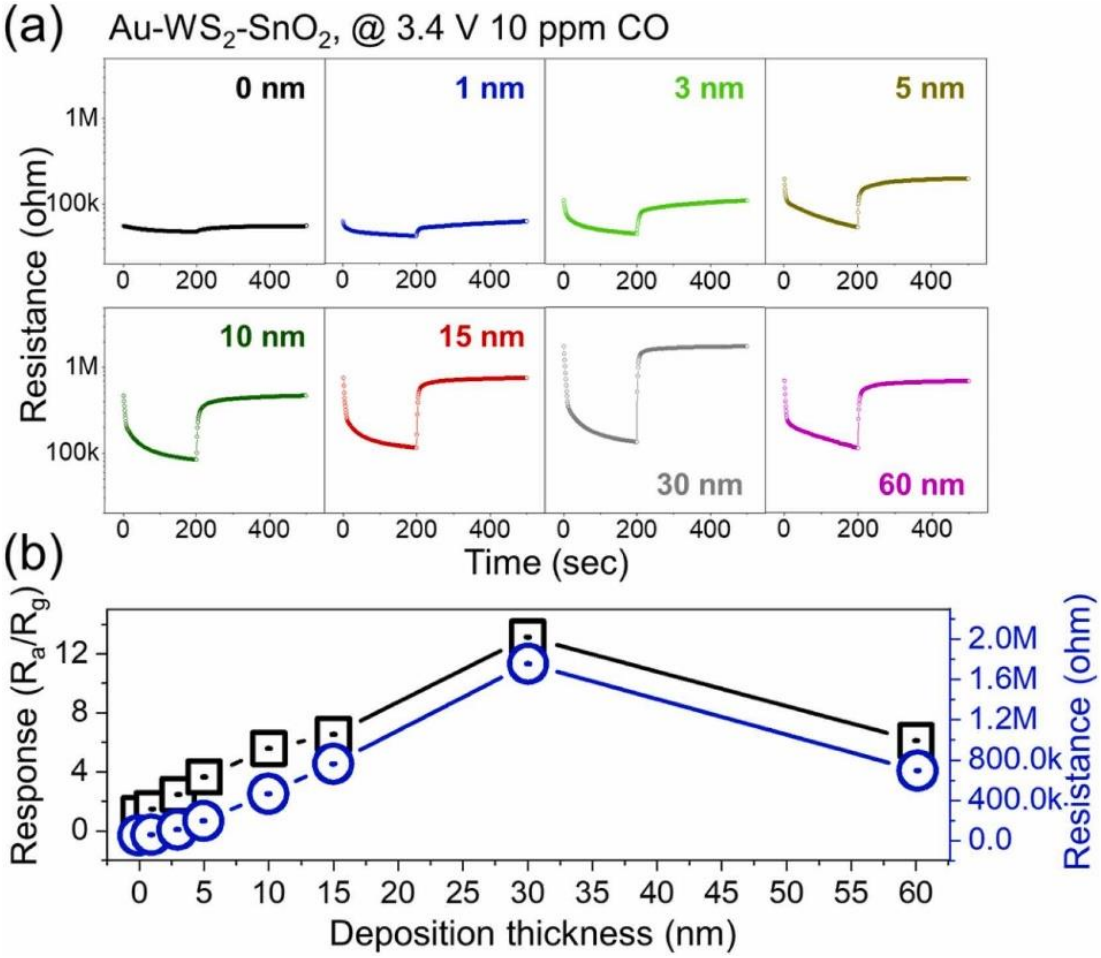

Figure 10. (**a**) Dynamic resistance plots of Au-decorated WS_2–SnO_2 C–S NS gas sensors with different shell thicknesses to 10 ppm of CO gas at 3.4 V. (**b**) Corresponding response and base resistance versus the shell thickness. Reprinted with permission from Ref. [112]. Copyright 2022, Elsevier.

As shown in Figure 11a,b, when the thickness of the shell is less, the entire shell is depleted of electrons in the air, and subsequent exposure to CO gas results in a significant modulation of the sensor resistance. Furthermore, as shown in Figure 11c, the formation of heterojunctions and modulation in the air and CO atmospheres contributes to the sensing signal. Figure 11d–f show the effects of Au and the shell thickness on the sensing performance. It can be concluded that the Au NPs have a positive catalytic effect on the gas-detection mechanism.

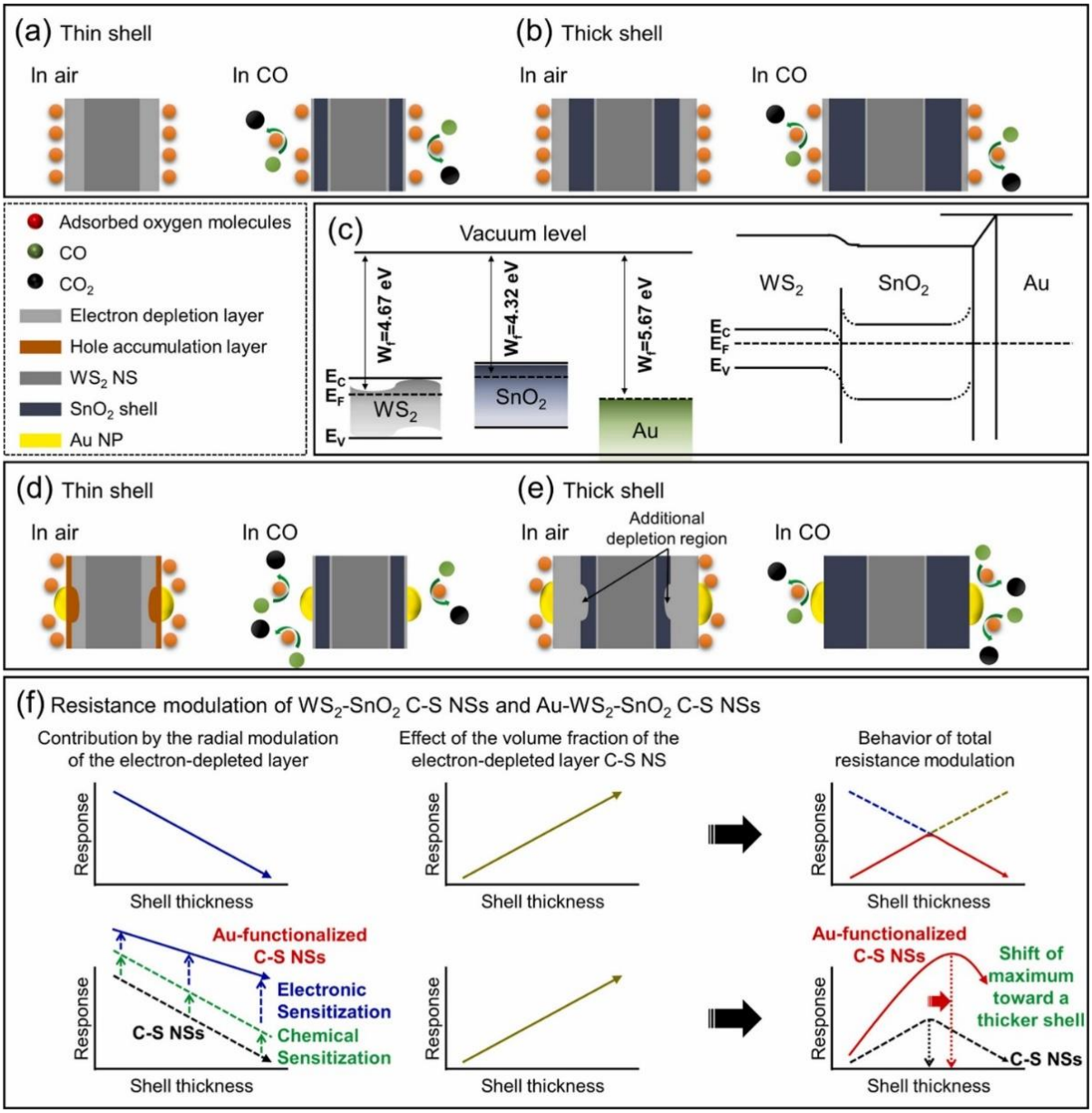

Figure 11. Gas-sensing mechanism of (**a**) thin-shell and (**b**) thick-shell pristine WS_2–SnO_2 core–shell NSs. (**c**) Energy bands of Au-functionalized WS_2–SnO_2 core–shell NSs before and after contact. Gas-sensing mechanism of (**d**) thin-shell and (**e**) thick-shell Au-decorated WS_2–SnO_2 core–shell NSs. (**f**) Resistance modulation of pristine and Au-decorated WS_2–SNO_2 core–shell NS gas sensors. Reprinted with permission from Ref. [112]. Copyright 2022, Elsevier.

2.7. Three-Dimensional MOS Gas Sensors

Hierarchical nanostructures with three-dimensional (3D) morphology are composed of zero-, one-, two-, and three-dimensional morphologies, such as nanorods, nanotubes, or nanosheets [22]. Hierarchical nanostructures with high surface area provide more adsorption sites for target gases. In addition, with pores or channels in their structure, the diffusion of gases is facilitated, resulting in better interaction of the target gas with deep parts of the sensing material [113]. Vapor-phase growth and hydrothermal techniques are the two most-used methods to synthesize hierarchical nanostructures [22]. Owing to these advantages, hierarchical morphologies of MOSs are widely used for sensing studies [114,115].

For instance, Guo et al. [116] used a 3D hierarchical hollow structure of CuO/WO_3 for p-xylene-sensing studies (Figure 12). The sensor showed a good response to 6.36–50 ppm of xylene gas at 260 °C. The sensing mechanism was related to the unique 3D hierarchical structure with a high surface area of 23.4962 $m^2 \cdot g^{-1}$, the formation of defects in the interfaces between CuO and WO_3, and the formation of p–n heterojunctions between CuO and WO_3. Recently, Yu et. al. [117] reviewed MOSs with hierarchical structures for gas-sensing studies.

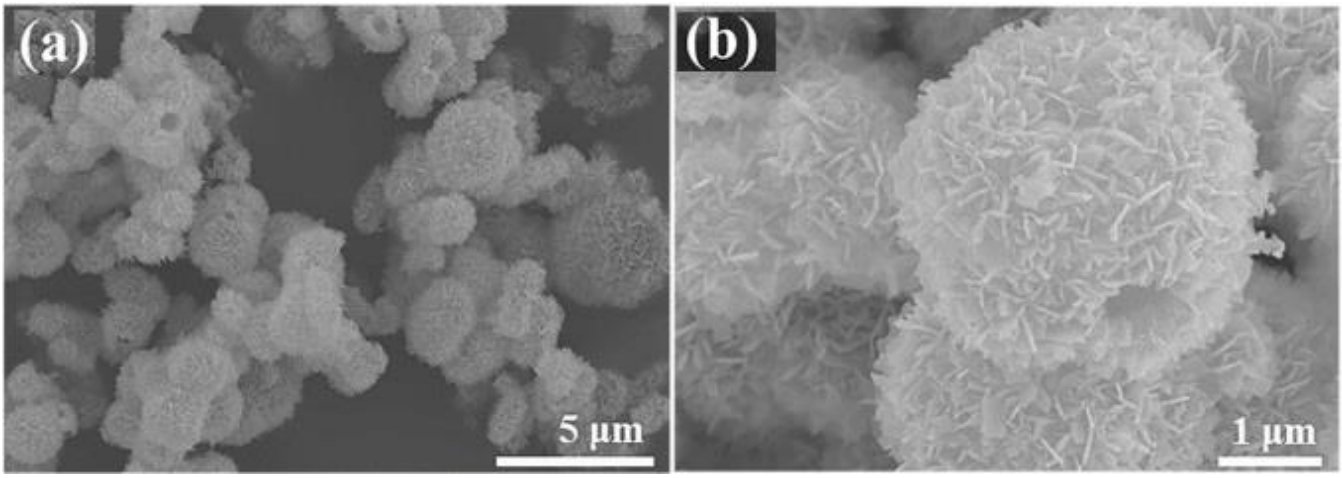

Figure 12. (**a**,**b**) SEM images of hierarchical CuO–WO_3 nanostructures at two different magnifications. Reprinted with permission from Ref. [116]. Copyright 2022, Elsevier.

2.8. Noble-Metal-Decorated MOS Gas Sensors

Gas-sensing properties can be improved by loading MOSs with small amounts of appropriately chosen noble metals. Noble metals such as Au, Pt, Pd, Ag, and Ru are widely used for the decoration or functionalization of the MOS surfaces to improve the overall performance of the resulting gas sensors. The basic properties of the prominent noble metals (i.e., Pt, Au, Pd, and Ag) are listed in Table 1 [118]. In particular, the work functions of Pt, Pd, Au, and Ag are approximately 5.65, 5.3, 5.1, and 4.3 eV, respectively.

Table 1. Properties of some noble metals [118]. Reprinted with permission from Ref. [118]. Copyright 2015, Elsevier.

Property	Pt	Pd	Au	Ag
Melting point (°C)	1769	1552	1064.4	961.9
Atomic number	78	46	79	47
Atomic mass (g/mol)	195.09	160.4	196.97	107.86
Density (g/cm^3)	21.45	12.02	19.30	10.49
Work function (eV)	~5.65	~5.3	~5.1	~4.3
Electron negativity	2.2	2.2	2.4	1.9

It should be noted that the noble metals need to be dispersed as finely as possible on the surface of the MOSs. Agglomeration of noble metals on the surface of the sensing layer can lead to a poor response of the gas sensor. Generally, noble metals affect the gas-sensing performance via two well-known mechanisms: The chemical sensitization mechanism, which occurs via the spillover effect, is a commonly known phenomenon in catalytic chemistry. In this case, the noble metal activates the target gas to facilitate catalytic oxidation of gas. Noble metals increase the gas sensitivity as they increase the rate of chemical processes [119]. In electronic sensitization, because noble metals generally have

a larger work function than MOSs, electrons are transferred from the MOS to the noble metals, leading to the formation of Schottky barriers and contraction of the EDL or HAL inside the MOS. In the target gas atmosphere, the width of the EDL and the HAL changes, leading to significant modulation of the sensor resistance. Among noble metals, Pd is well known for H_2 gas detection [120], owing to its excellent catalytic activation ability for hydrogen through the hydrogen spillover effect [121]. When a sensor decorated with Pd NPs is placed in an atmosphere containing H_2 molecules, hydrogen can easily dissociate into hydrogen atoms on the Pd surface; in the spillover effect, hydrogen atoms move to the neighboring MOS surfaces, leading to additional reactions between atomic hydrogen and adsorbed oxygen [122]. Other noble metals also exhibit good catalytic activities toward different gases. For example, Ag is often used for H_2S detection because of the generation of Ag_2S upon exposure to H_2S gas [123]. Pt and Pd also have good catalytic activities toward C_7H_8 and C_6H_6 gases, respectively [124,125].

2.9. Hybrid MOS Gas Sensors

A good strategy to enhance the gas-sensing characteristics of MOS-based gas sensors is using another material in combination with the MOS. Hybrid MOS nanocomposites are either (i) composites of MOS and carbon materials such as graphene, graphene oxide (GO), reduced graphene oxide (rGO), and carbon nanotubes, or (ii) composites of MOS and conductive polymers (CPs). Graphene, which comprises sp^2 carbon atoms, is utilized in gas sensors due to its high charge carrier mobility (200,000 $cm^2\ V^{-1}\ s^{-1}$) and large surface area (2630 $m^2\ g^{-1}$) [126]. The first ever graphene gas sensor was introduced in 2007 [127]. Owing to its single-layer or few-layer nature, graphene can even interact with a single molecule. Pristine graphene can easily agglomerate owing to the surface interactions. Furthermore, graphene has no band gap, hindering its gas-sensing usage [128]. Thus, rGO, with its many functional groups—such as -OH and –O—as well as defects, is a better choice for gas-sensing studies. Although GO can be used for sensing applications, it has a very high resistance owing to the presence of oxygen-based functional groups, limiting its use in sensing studies [129]. rGO can be synthesized from GO using chemical reduction, thermal reduction, and UV light reduction methods [130,131]. Many papers on gas sensors with hybrids of MOSs and carbon allotropes have been reported. However, for sensing studies, rGO is the most effective allotrope of carbon in its hybrid form. This is because of its large surface area, presence of many defects, and high concentrations of charge carriers with high mobility—all of which are beneficial for sensing. Accordingly, several studies have been reported on hybrid MOS–rGO composites with the ability to operate at room temperature [132,133].

CPs have tunable conductivity and high flexibility in synthesis and processing. However, because of the high affinity of CPs for moisture, they are unstable, and generally exhibit poor sensitivity and selectivity for different gases in their pristine form. The use of hybrid nanocomposites with CPs and MOSs could result in the development of room-temperature gas sensors [134]. Accordingly, hybrids of CPs and MOSs have been used to enhance the sensitivity of nanostructured sensors at low or room temperature [135,136]. One application of hybrids of MOSs and CPs is the development of flexible and wearable gas sensors. Flexible gas sensors are generally deposited on flexible substrates, and need to work at low temperatures, e.g., room temperature. Since composites of MOs and CPs can function at low temperatures, they are good candidates for such applications.

2.10. Comparison of Performance of Gas Sensors with Different Morphologies

Table 2 summarizes the performance of gas sensors with various morphologies. Different morphologies and compositions have been used for the detection of various gases at different temperatures. Moreover, pristine gas sensors show lower responses and higher sensing temperatures, while composite or decorated sensing materials show better performance at lower temperatures.

Table 2. Gas-sensing properties of different sensors with various morphologies.

Sensing Material	Morphology	Gas	Conc. (ppm)	T (°C)	Response (R_a/R_g) or (R_g/R_a)	Ref.
TiO_2/SnO_2	QD	NO_2	1	300	2.62	[25]
SnO_2	QD	C_4H_{10}	8219.2	25	8.09	[26]
SnO_2	QD	C_2H_5OH	300	N/A *	215	[27]
Pt-SnO_2	NW	C_7H_8	100	300	55	[32]
In_2O_3/SnO_2	NW	NO_2	5	300	25	[34]
In_2O_3	NR	CO	400	350	3.5	[35]
SnO_2	NW	NO_2	5	200	180	[36]
SnO_2	NW	LPG	2000	350	21.8	[37]
SnO_2	NW	H_2	1000	300	3.3	[42]
ZnO	NW	NO_2	20	225	95	[43]
SnO_2	NW	C_2H_5OH	100	300	50.6	[48]
ZnO	NW	NO_2	5	300	106	[49]
ZnO-SnO_2	NR	C_2H_5OH	100	275	18	[50]
Ni/ZnO	NW	p-xylene	5	400	42.44	[52]
Gr/ZnO	NW	C_2H_5OH	20	125	23	[53]
Bi_2O_3/SnO_2	NW	NO_2	2	250	56.92	[54]
Pt/CeO_2	NW	CO	200	25	3	[56]
SnO_2	NW	NO_2	500	300	17	[57]
SnO_2	NW	C_2H_5OH	50	350	6.7	[58]
NiO/$NiFe_2O_4$	Nanotetrahedrons	HCHO	50	240	19	[61]
ZnO/SnO_2	NW	C_2H_5OH	200	400	280	[62]
$ZnGa_2O_4$/ZnO	NW	NO_2	10	250	23	[63]
ZnO/WO_3	NW	H_2	1000	25	6.45	[64]
Ga_2O_3/SnO_2	NW	C_2H_5OH	1000	400	66	[65]
Au/SnO_2–ZnO	NW	CO	0.1	300	26.6	[67]
Pt/$W_{18}O_{49}$	NW	H_2	1000	200	0.528	[70]
Ag/SnO_2	NW	H_2S	0.5	N/A *	21.2	[73]
Rh/SnO_2	NF	C_3H_6O	50	200	60.6	[78]
ZnO/In_2O_3	NF	C_2H_5OH	100	225	31.87	[85]
SnO_2/Cu_2O	NF	NO_2	10	300	5	[87]
In_2O_3	NF	CO	100	300	5.4	[89]
Pd/SnO_2	NF	HCHO	100	160	18.8	[92]
Co_3O_4/ZnO	NF	HCHO	100	220	5	[93]
TiO_2/ZnO	Hemitube	NO_2	25	25	1.23	[98]
ZnO	NR	NO_2	5	250	200	[100]
ZnO	NR	C_2H_5OH	250	400	7	[101]
α-Ag_2WO_4	NR	C_3H_6O	20	350	3.6	[103]
ZnO	NR	O_3	2.5	575	850	[106]
ZnO	NS	NO_2	10	200	74.68	[111]

* N/A: No available data.

3. Conclusions and Outlooks

MOS-based gas sensors are popular for different applications because of their high sensing performance and low cost of synthesis and fabrication. Many MOSs can be utilized for the production of gas sensors; however, most studies deal with n-type MOSs—especially SnO_2 and ZnO materials. There are many techniques to synthesize sensing materials with different morphologies. One of the most popular techniques for the synthesis of MOS NWs and branched NWs is the vapor–liquid–solid technique. In this technique, by controlling the gas flow, furnace temperature, time, and catalyst, it is possible to achieve extremely long MOS NWs. Electrospinning is mainly used for the synthesis of MOSs with NF morphology. In this technique, by controlling the feeding rate, applied voltage, solution viscosity, needle-to-collector distance, and temperature, it is possible to control the morphology. In this way, the creation of very long and rough NFs is possible. The ALD technique has been successfully used to deposit a shell over a core. In this technique, by adjusting the ALD cycles, it is possible to control the thickness of the shell layer. MOS NTs

are mainly synthesized using a soft core; after synthesis, the core is removed, and a hollow structure remains. In this technique, choosing an appropriate soft core and annealing temperature to remove the core are key factors determining the hollowness of the structure. Chemical methods such as hydrothermal and sol–gel methods are used for the fabrications of NSs, NRs, and hierarchical structures. In these techniques, appropriate choices of the concentration of the solution, annealing temperature, time, and pH are important to obtain the best morphology.

Various morphologies of MOS-based gas sensors—such as QDs, NWs, NFs, NTs, NRs, NS, and hierarchical structures—have been fabricated for sensing applications, with the goal of increasing the active surface of the resulting gas sensor. Furthermore, C–S structures with NW or NS morphology have been extensively investigated, wherein an optimal shell with the highest sensing performance was employed. NSs with 2D morphology offer a high surface area for incoming gas molecules. However, owing to the presence of surface forces, they are generally bonded together, which may decrease their sensing performance. Hierarchical nanostructures are also promising for sensor fabrication. With the ease of synthesis and high response, they are among the best materials for sensing studies. The effects of different noble metals—such as Au, Ag, Pt, and Pd—on MOS gas sensors have also been extensively studied. Noble metals promote sensing performance through both chemical and electronic sensitization effects. However, uniform dispersion on the surface and optimization of the amounts are necessary to achieve optimal performance. A hybrid MOS with carbon and polymer materials can remarkably reduce power consumption and enable operation at low temperatures. Another strategy is the use of a sensor in self-heating mode to reduce power consumption.

Future directions for this research can include the production of novel morphologies and combinations of 1D, 2D, and 3D materials with high surface area and high porosity. For example, there is limited literature on the synthesis of 1D/2D composite materials for sensing studies. Moreover, the combination of two noble metals on the surface of an MOS can be used to increase the sensor response and the dynamics of the sensor, such as the response and recovery times. Finding optimal composites of MOSs, carbon nanomaterials, or CPs could lead to high-performance gas sensors suitable for low-temperature operation. Composites with novel sensing materials such as MXenes, transition metal dichalcogenides, and metal–organic frameworks can provide many opportunities to decrease the sensing temperature, increase the response to target gases, and improve the selectivity of MOS-based gas sensors. The integration of gas sensors into low-power-consumption and portable electronic devices such as smartphones needs further development of MOS-based gas sensors in terms of reduction in sensing temperature, increase in response, and selectivity.

Author Contributions: Conceptualization, A.M., H.W.K. and S.S.K.; investigation, A.M., H.R.A. and J.-Y.K.; writing—original draft preparation, A.M., H.W.K., M.S. and S.S.K.; writing—review and editing, A.M., H.W.K. and S.S.K.; supervision, H.W.K. and S.S.K. All authors have read and agreed to the published version of the manuscript.

Funding: This research received no external funding.

Institutional Review Board Statement: Not applicable.

Informed Consent Statement: Not applicable.

Acknowledgments: This research was supported by Inha University.

Conflicts of Interest: The authors declare no conflict of interest.

References

1. Kampa, M.; Castanas, E. Human health effects of air pollution. *Environ. Pollut.* **2008**, *151*, 362–367. [CrossRef] [PubMed]
2. Paralovo, S.L.; Barbosa, C.G.G.; Carneiro, I.P.S.; Kurzlop, P.; Borillo, G.C.; Schiochet, M.F.C.; Godoi, A.F.L.; Yamamoto, C.I.; de Souza, R.A.F.; Andreoli, R.V. Observations of particulate matter, NO_2, SO_2, O_3, H_2S and selected VOCs at a semi-urban environment in the Amazon region. *Sci. Total Environ.* **2019**, *650*, 996–1006. [CrossRef] [PubMed]
3. Jung, S.J.; Mehta, J.S.; Tong, L. Effects of environment pollution on the ocular surface. *Ocul. Surf.* **2018**, *16*, 198–205. [CrossRef]

4. Elizabeth, F.Y.; Kenneth, Z.; Naus, A.; Forbes, C.; Wu, X.; Dey, T. A review on the biological, epidemiological, and statistical relevance of COVID-19 paired with air pollution. *Environ. Adv.* **2022**, *8*, 100250.
5. Li, X.; Li, Y. The impact of perceived air pollution on labour supply: Evidence from China. *J. Environ. Manag.* **2022**, *306*, 114455. [CrossRef] [PubMed]
6. Brauer, M.; Casadei, B.; Harrington, R.A.; Kovacs, R.; Sliwa, K.; The WHF Air Pollution Expert Group. Taking a stand against air pollution—The impact on cardiovascular disease: A joint opinion from the World Heart Federation, American College of Cardiology, American Heart Association, and the European Society of Cardiology. *Circulation* **2021**, *143*, e800–e804. [CrossRef]
7. Khuda, K.E. Air Pollution in the Capital City of Bangladesh: Its Causes and Impacts on Human Health. *Pollution* **2020**, *6*, 737–750.
8. Ming, Y.; Deng, H.; Wu, X. The negative effect of air pollution on people's pro-environmental behavior. *J. Bus. Res.* **2022**, *142*, 72–87. [CrossRef]
9. Mirzaei, A.; Lee, J.-H.; Majhi, S.M.; Weber, M.; Bechelany, M.; Kim, H.W.; Kim, S.S. Resistive gas sensors based on metal-oxide nanowires. *J. Appl. Phys.* **2019**, *126*, 241102. [CrossRef]
10. Pifferi, S.; Menini, A. Odorant detection and discrimination in the olfactory system. *Sens. Microsyst.* **2011**, *91*, 3–18.
11. Kotecha, A.M.; Corrêa, A.D.C.; Fisher, K.M.; Rushworth, J.V. Olfactory dysfunction as a global biomarker for sniffing out Alzheimer's disease: A meta-analysis. *Biosensors* **2018**, *8*, 41. [CrossRef] [PubMed]
12. White, L.T. *Hazardous Gas Monitoring: A Guide for Semiconductor and Other Hazardous Occupancies*; William Andrew: New York, NY, USA, 2001; ISBN 081551784X.
13. Brattain, W.H.; Bardeen, J. Surface properties of germanium. *Bell Syst. Tech. J.* **1953**, *32*, 1–41. [CrossRef]
14. Heiland, G. Zum Einfluß von adsorbiertem Sauerstoff auf die elektrische Leitfähigkeit von Zinkoxydkristallen. *Z. Phys.* **1954**, *138*, 459–464. [CrossRef]
15. Seiyama, T.; Kato, A.; Fujiishi, K.; Nagatani, M. A new detector for gaseous components using semiconductive thin films. *Anal. Chem.* **1962**, *34*, 1502–1503. [CrossRef]
16. Shaver, P.J. Activated tungsten oxide gas detectors. *Appl. Phys. Lett.* **1967**, *11*, 255–257. [CrossRef]
17. Taguchi, N. Gas-Detecting Device. U.S. Patent 3,631,436, 28 December 1971.
18. Korotcenkov, G. Metal oxides for solid-state gas sensors: What determines our choice? *Mater. Sci. Eng. B* **2007**, *139*, 1–23. [CrossRef]
19. Yamazoe, N.; Sakai, G.; Shimanoe, K. Oxide semiconductor gas sensors. *Catal. Surv. Asia* **2003**, *7*, 63–75. [CrossRef]
20. Quan, W.; Hu, X.; Min, X.; Qiu, J.; Tian, R.; Ji, P.; Qin, W.; Wang, H.; Pan, T.; Cheng, S. A highly sensitive and selective ppb-level acetone sensor based on a Pt-doped 3D porous SnO_2 hierarchical structure. *Sensors* **2020**, *20*, 1150. [CrossRef]
21. Korotcenkov, G. The role of morphology and crystallographic structure of metal oxides in response of conductometric-type gas sensors. *Mater. Sci. Eng. R Rep.* **2008**, *61*, 1–39. [CrossRef]
22. Kim, H.-J.; Lee, J.-H. Highly sensitive and selective gas sensors using p-type oxide semiconductors: Overview. *Sens. Actuators B Chem.* **2014**, *192*, 607–627. [CrossRef]
23. Vardan, G. Quantum dots: Perspectives in next-generation chemical gas sensors—A review. *Anal. Chim. Acta* **2021**, *1152*, 238192.
24. Chen, D.; Huang, S.; Huang, R.; Zhang, Q.; Le, T.T.; Cheng, E.; Hu, Z.; Chen, Z. Highlights on advances in SnO_2 quantum dots: Insights into synthesis strategies, modifications and applications. *Mat. Res. Lett.* **2018**, *6*, 462–488. [CrossRef]
25. Lee, J.-H.; Mirzaei, A.; Kim, J.H.; Kim, J.-Y.; Nasriddinov, A.F.; Marina Rumyantseva, N.; Kim, H.W.; Kim, S.S. Gas-sensing behaviors of TiO_2-layer-modified SnO_2 quantum dots in self-heating mode and effects of the TiO_2 layer. *Sens. Actuators B-Chem.* **2020**, *310*, 127870. [CrossRef]
26. Liu, J.; Lv, J.; Xiong, H.; Wang, Y.; Jin, G.; Zhai, Z.; Fu, C.; Zhang, Q. Size effect and comprehensive mathematical model for gas-sensing mechanism of SnO_2 thin film gas sensors. *J. Alloys Compd.* **2022**, *898*, 162875. [CrossRef]
27. Zhu, L.; Wang, M.; Lam, T.K.; Zhang, C.; Du, H.; Li, B.; Yao, Y. Fast microwave-assisted synthesis of gas-sensing SnO_2 quantum dots with high sensitivity. *Sens. Actuators B-Chem.* **2016**, *236*, 646–653. [CrossRef]
28. Murphy, C.J.; Jana, N.R. Controlling the aspect ratio of inorganic nanorods and nanowires. *Adv. Mater.* **2002**, *14*, 80–82. [CrossRef]
29. Comini, E.; Sberveglieri, G. Metal oxide nanowires as chemical sensors. *Mater. Today* **2010**, *13*, 36–44. [CrossRef]
30. Ramgir, N.; Datta, N.; Kaur, M.; Kailasaganapathi, S.; Debnath, A.K.; Aswal, D.K.; Gupta, S.K. Metal oxide nanowires for chemiresistive gas sensors: Issues, challenges and prospects. *Colloids Surf. A Physicochem. Eng. Asp.* **2013**, *439*, 101–116. [CrossRef]
31. Yuan, K.; Wang, C.-Y.; Zhu, L.-Y.; Cao, Q.; Yang, J.-H.; Li, X.-X.; Huang, W.; Wang, Y.-Y.; Lu, H.-L.; Zhang, D.W. Fabrication of a micro-electromechanical system-based acetone gas sensor using CeO_2 nanodot-decorated WO_3 nanowires. *ACS Appl. Mater. Interfaces* **2020**, *12*, 14095–14104. [CrossRef]
32. Tonezzer, M.; Kim, J.-H.; Lee, J.-H.; Iannotta, S.; Kim, S.S. Predictive gas sensor based on thermal fingerprints from Pt-SnO_2 nanowires. *Sens. Actuators B Chem.* **2019**, *281*, 670–678. [CrossRef]
33. Galstyan, V.; Moumen, A.; Kumarage, G.W.; Comini, E. Progress towards chemical gas sensors: Nanowires and 2D semiconductors. *Sens. Actuators B-Chem.* **2022**, *357*, 131466. [CrossRef]
34. Park, S.; Jung, Y.W.; Ko, G.M.; Jeong, D.Y.; Lee, C. Enhanced NO_2 gas sensing performance of the In_2O_3-decorated SnO_2 nanowire sensor. *Appl. Phys. A* **2021**, *127*, 898. [CrossRef]
35. Van Tong, P.; Minh, L.H.; Van Duy, N.; Hung, C.M. Porous In_2O_3 nanorods fabricated by hydrothermal method for an effective CO gas sensor. *Mater. Res. Bull.* **2021**, *137*, 111179. [CrossRef]
36. Choi, Y.-J.; Hwang, I.-S.; Park, J.-G.; Choi, K.J.; Park, J.-H.; Lee, J.-H. Novel fabrication of an SnO_2 nanowire gas sensor with high sensitivity. *Nanotechnology* **2008**, *19*, 95508. [CrossRef] [PubMed]

37. Hoa, N.D.; Le, D.T.T.; Tam, P.D.; Le, A.-T.; Van Hieu, N. On-chip fabrication of SnO_2-nanowire gas sensor: The effect of growth time on sensor performance. *Sens. Actuators B Chem.* **2010**, *146*, 361–367.
38. Arlinghaus, F.J. Energy bands in stannic oxide (SnO_2). *J. Phys. Chem. Solids* **1974**, *35*, 931–935. [CrossRef]
39. Yadav, K.K.; Guchhait, S.K.; Sood, K.; Mehta, S.K.; Ganguli, A.K.; Jha, M. Mechanistic insights of enhanced photocatalytic efficiency of SnO_2-SnS_2 heterostructures derived from partial sulphurization of SnO_2. *Sep. Purif. Technol.* **2020**, *242*, 116835.
40. Gondal, M.A.; Drmosh, Q.A.; Saleh, T.A. Preparation and characterization of SnO_2 nanoparticles using high power pulsed laser. *Appl. Surf. Sci.* **2010**, *256*, 7067–7070. [CrossRef]
41. Das, S.; Jayaraman, V. SnO_2: A comprehensive review on structures and gas sensors. *Prog. Mater. Sci.* **2014**, *66*, 112–255. [CrossRef]
42. Wang, B.; Zhu, L.F.; Yang, Y.H.; Xu, N.S.; Yang, G.W. Fabrication of a SnO_2 nanowire gas sensor and sensor performance for hydrogen. *J. Phys. Chem. C* **2008**, *112*, 6643–6647. [CrossRef]
43. Ahn, M.-W.; Park, K.-S.; Heo, J.-H.; Park, J.-G.; Kim, D.-W.; Choi, K.J.; Lee, J.-H.; Hong, S.-H. Gas sensing properties of defect-controlled ZnO-nanowire gas sensor. *Appl. Phys. Lett.* **2008**, *93*, 263103. [CrossRef]
44. Yi, S.; Tian, S.; Zeng, D.; Xu, K.; Zhang, S.; Xie, C. An In_2O_3 nanowire-like network fabricated on coplanar sensor surface by sacrificial CNTs for enhanced gas sensing performance. *Sens. Actuators B Chem.* **2013**, *185*, 345–353. [CrossRef]
45. Kaur, N.; Zappa, D.; Maraloiu, V.; Comini, E. Novel Christmas Branched Like $NiO/NiWO_4/WO_3$ (p–p–n) Nanowire Heterostructures for Chemical Sensing. *Adv. Funct. Mater.* **2021**, *31*, 2104416. [CrossRef]
46. Liu, H.; Wang, Z.; Cao, G.; Pan, G.; Yang, X.; Qiu, M.; Sun, C.; Shao, J.; Li, Z.; Zhang, H. Construction of hollow NiO/ZnO pn heterostructure for ultrahigh performance toluene gas sensor. *Mater. Sci. Semicond. Process.* **2022**, *141*, 106435. [CrossRef]
47. Cheng, C.; Fan, H.J. Branched nanowires: Synthesis and energy applications. *Nano Today* **2012**, *7*, 327–343. [CrossRef]
48. Wan, Q.; Huang, J.; Xie, Z.; Wang, T.; Dattoli, E.N.; Lu, W. Branched SnO_2 nanowires on metallic nanowire backbones for ethanol sensors application. *Appl. Phys. Lett.* **2008**, *92*, 102101. [CrossRef]
49. An, S.; Park, S.; Ko, H.; Jin, C.; Lee, W.I.; Lee, C. Enhanced gas sensing properties of branched ZnO nanowires. *Thin Solid Film.* **2013**, *547*, 241–245. [CrossRef]
50. Yang, X.; Zhang, S.; Zhao, L.; Sun, P.; Wang, T.; Liu, F.; Yan, X.; Gao, Y.; Liang, X.; Zhang, S. One step synthesis of branched SnO_2/ZnO heterostructures and their enhanced gas-sensing properties. *Sens. Actuators B Chem.* **2019**, *281*, 415–423. [CrossRef]
51. Wang, Y.; Zhou, Y.; Meng, C.; Gao, Z.; Cao, X.; Li, X.; Xu, L.; Zhu, W.; Peng, X.; Zhang, B. A high-response ethanol gas sensor based on one-dimensional TiO_2/V_2O_5 branched nanoheterostructures. *Nanotechnology* **2016**, *27*, 425503. [CrossRef]
52. Woo, H.-S.; Kwak, C.-H.; Chung, J.-H.; Lee, J.-H. Highly selective and sensitive xylene sensors using Ni-doped branched ZnO nanowire networks. *Sens. Actuators B Chem.* **2015**, *216*, 358–366. [CrossRef]
53. Rafiee, Z.; Roshan, H.; Sheikhi, M.H. Low concentration ethanol sensor based on graphene/ZnO nanowires. *Ceram. Int.* **2021**, *47*, 5311–5317. [CrossRef]
54. Bang, J.H.; Choi, M.S.; Mirzaei, A.; Kwon, Y.J.; Kim, S.S.; Kim, T.W.; Kim, H.W. Selective NO_2 sensor based on Bi_2O_3 branched SnO_2 nanowires. *Sens. Actuators B Chem.* **2018**, *274*, 356–369. [CrossRef]
55. Afshar, M.; Preiß, E.M.; Sauerwald, T.; Rodner, M.; Feili, D.; Straub, M.; König, K.; Schütze, A.; Seidel, H. Indium-tin-oxide single-nanowire gas sensor fabricated via laser writing and subsequent etching. *Sens. Actuators B Chem.* **2015**, *215*, 525–535. [CrossRef]
56. Liao, L.; Mai, H.X.; Yuan, Q.; Lu, H.B.; Li, J.C.; Liu, C.; Yan, C.H.; Shen, Z.X.; Yu, T. Single CeO_2 nanowire gas sensor supported with Pt nanocrystals: Gas sensitivity, surface bond states, and chemical mechanism. *J. Phys. Chem. C* **2008**, *112*, 9061–9065. [CrossRef]
57. Tonezzer, M.; Hieu, N.V. Size-dependent response of single-nanowire gas sensors. *Sens. Actuators B Chem.* **2012**, *163*, 146–152. [CrossRef]
58. Tonezzer, M. Selective gas sensor based on one single SnO_2 nanowire. *Sens. Actuators B Chem.* **2019**, *288*, 53–59. [CrossRef]
59. Czaban, J.A.; Thompson, D.A.; LaPierre, R.R. GaAs core−shell nanowires for photovoltaic applications. *Nano Lett.* **2009**, *9*, 148–154. [CrossRef]
60. Kim, J.H.; Mirzaei, A.; Kim, H.W.; Kim, S.S. Variation of shell thickness in ZnO-SnO_2 core-shell nanowires for optimizing sensing behaviors to CO, C_6H_6, and C_7H_8 gases. *Sens. Actuators B-Chem.* **2020**, *302*, 127150. [CrossRef]
61. Xu, Y.; Tian, X.; Fan, Y.; Sun, Y. A formaldehyde gas sensor with improved gas response and sub-ppm level detection limit based on $NiO/NiFe_2O_4$ composite nanotetrahedrons. *Sens. Actuators B Chem.* **2020**, *309*, 127719. [CrossRef]
62. Hwang, I.-S.; Kim, S.-J.; Choi, J.-K.; Choi, J.; Ji, H.; Kim, G.-T.; Cao, G.; Lee, J.-H. Synthesis and gas sensing characteristics of highly crystalline ZnO–SnO_2 core–shell nanowires. *Sens. Actuators B Chem.* **2010**, *148*, 595–600. [CrossRef]
63. Chen, I.; Lin, S.-S.; Lin, T.-J.; Hsu, C.-L.; Hsueh, T.J.; Shieh, T.-Y. The assessment for sensitivity of a NO_2 gas sensor with $ZnGa_2O_4/ZnO$ core-shell nanowires—A novel approach. *Sensors* **2010**, *10*, 3057–3072. [CrossRef] [PubMed]
64. Park, S.; Hong, T.; Jung, J.; Lee, C. Room temperature hydrogen sensing of multiple networked ZnO/WO_3 core–shell nanowire sensors under UV illumination. *Curr. Appl. Phys.* **2014**, *14*, 1171–1175. [CrossRef]
65. Jang, Y.-G.; Kim, W.-S.; Kim, D.-H.; Hong, S.-H. Fabrication of Ga_2O_3/SnO_2 core–shell nanowires and their ethanol gas sensing properties. *J. Mater. Res.* **2011**, *26*, 2322–2327. [CrossRef]
66. Mirzaei, A.; Kim, J.-H.; Kim, H.W.; Kim, S.S. How shell thickness can affect the gas sensing properties of nanostructured materials: Survey of literature. *Sens. Actuators B Chem.* **2018**, *258*, 270–294. [CrossRef]

67. Kim, J.H.; Mirzaei, A.; Kim, H.W.; Kim, S.S. Extremely sensitive and selective sub-ppm CO detection by the synergistic effect of Au nanoparticles and core–shell nanowires. *Sens. Actuators B-Chem.* **2017**, *249*, 177–188. [CrossRef]
68. Salehi, A. A highly sensitive self heated SnO_2 carbon monoxide sensor. *Sens. Actuators B Chem.* **2003**, *96*, 88–93. [CrossRef]
69. Fàbrega, C.; Casals, O.; Hernández-Ramírez, F.; Prades, J.D. A review on efficient self-heating in nanowire sensors: Prospects for very-low power devices. *Sens. Actuators B Chem.* **2018**, *256*, 797–811. [CrossRef]
70. Zhu, L.F.; She, J.C.; Luo, J.Y.; Deng, S.Z.; Chen, J.; Ji, X.W.; Xu, N.S. Self-heated hydrogen gas sensors based on Pt-coated $W_{18}O_{49}$ nanowire networks with high sensitivity, good selectivity and low power consumption. *Sens. Actuators B Chem.* **2011**, *153*, 354–360. [CrossRef]
71. Majhi, S.M.; Mirzaei, A.; Kim, H.W.; Kim, S.S.; Kim, T.W. Recent advances in energy-saving chemiresistive gas sensors: A review. *Nano Energy* **2021**, *79*, 105369. [CrossRef]
72. Ngoc, T.M.; Van Duy, N.; Hung, C.M.; Hoa, N.D.; Trung, N.N.; Nguyen, H.; Van Hieu, N. Ultralow power consumption gas sensor based on a self-heated nanojunction of SnO_2 nanowires. *RSC Adv.* **2018**, *8*, 36323–36330. [CrossRef]
73. Ngoc, T.M.; Van Duy, N.; Hoa, N.D.; Hung, C.M.; Nguyen, H.; Van Hieu, N. Effective design and fabrication of low-power-consumption self-heated SnO_2 nanowire sensors for reducing gases. *Sens. Actuators B Chem.* **2019**, *295*, 144–152. [CrossRef]
74. Ngoc, T.M.; Van Duy, N.; Hung, C.M.; Hoa, N.D.; Nguyen, H.; Tonezzer, M.; Van Hieu, N. Self-heated Ag-decorated SnO_2 nanowires with low power consumption used as a predictive virtual multisensor for H_2S-selective sensing. *Anal. Chim. Acta* **2019**, *1069*, 108–116. [CrossRef] [PubMed]
75. Kim, J.-H.; Mirzaei, A.; Kim, H.W.; Kim, S.S. Low-voltage-driven sensors based on ZnO nanowires for room-temperature detection of NO_2 and CO gases. *ACS Appl. Mater. Interfaces* **2019**, *11*, 24172–24183. [CrossRef] [PubMed]
76. Kim, J.-H.; Mirzaei, A.; Bang, J.H.; Kim, H.W.; Kim, S.S. Selective H_2S sensing without external heat by a synergy effect in self-heated CuO-functionalized SnO_2-ZnO core-shell nanowires. *Sens. Actuators B Chem.* **2019**, *300*, 126981. [CrossRef]
77. Kim, J.-H.; Mirzaei, A.; Kim, H.W.; Kim, S.S. Pd-functionalized core-shell composite nanowires for self-heating, sensitive, and benzene-selective gas sensors. *Sens. Actuators A Phys.* **2020**, *308*, 112011. [CrossRef]
78. Kou, X.; Xie, N.; Chen, F.; Wang, T.; Guo, L.; Wang, C.; Wang, Q.; Ma, J.; Sun, Y.; Zhang, H. Superior acetone gas sensor based on electrospun SnO_2 nanofibers by Rh doping. *Sens. Actuators B Chem.* **2018**, *256*, 861–869. [CrossRef]
79. Li, Y.; Zhu, J.; Cheng, H.; Li, G.; Cho, H.; Jiang, M.; Gao, Q.; Zhang, X. Developments of advanced electrospinning techniques: A critical review. *Adv. Mater. Technol.* **2021**, *6*, 2100410. [CrossRef]
80. Rodríguez-Tobías, H.; Morales, G.; Grande, D. Comprehensive review on electrospinning techniques as versatile approaches toward antimicrobial biopolymeric composite fibers. *Mater. Sci. Eng. C* **2019**, *101*, 306–322. [CrossRef]
81. Abideen, Z.U.; Kim, J.-H.; Lee, J.-H.; Kim, J.-Y.; Mirzaei, A.; Kim, H.W.; Kim, S.S. Electrospun metal oxide composite nanofibers gas sensors: A review. *J. Korean Ceram. Soc.* **2017**, *54*, 366–379. [CrossRef]
82. Islam, M.S.; Ang, B.C.; Andriyana, A.; Afifi, A.M. A review on fabrication of nanofibers via electrospinning and their applications. *SN Appl. Sci.* **2019**, *1*, 1–16. [CrossRef]
83. Haider, A.; Haider, S.; Kang, I.-K. A comprehensive review summarizing the effect of electrospinning parameters and potential applications of nanofibers in biomedical and biotechnology. *Arab. J. Chem.* **2018**, *11*, 1165–1188. [CrossRef]
84. Tsai, P.; Chen, J.; Ercan, E.; Chueh, C.; Tung, S.; Chen, W. Uniform luminous perovskite nanofibers with color-tunability and improved stability prepared by one-step core/shell electrospinning. *Small* **2018**, *14*, 1704379. [CrossRef]
85. Huang, B.; Zhang, Z.; Zhao, C.; Cairang, L.; Bai, J.; Zhang, Y.; Mu, X.; Du, J.; Wang, H.; Pan, X. Enhanced gas-sensing performance of ZnO@ In_2O_3 core@ shell nanofibers prepared by coaxial electrospinning. *Sens. Actuators B Chem.* **2018**, *255*, 2248–2257. [CrossRef]
86. Ding, B.; Wang, M.; Yu, J.; Sun, G. Gas sensors based on electrospun nanofibers. *Sensors* **2009**, *9*, 1609–1624. [CrossRef] [PubMed]
87. Kim, J.H.; Lee, J.H.; Kim, J.Y.; Mirzaei, A.; Kim, H.W.; Kim, S.S. Enhancement of CO and NO_2 sensing in n-SnO_2-p-Cu_2O core-shell nanofibers by shell optimization. *J. Hazard. Mater.* **2019**, *376*, 68–82. [CrossRef] [PubMed]
88. Kim, J.-H.; Lee, J.-H.; Mirzaei, A.; Kim, H.W.; Kim, S.S. Optimization and gas sensing mechanism of n-SnO_2-p-Co_3O_4 composite nanofibers. *Sens. Actuators B Chem.* **2017**, *248*, 500–511. [CrossRef]
89. Lim, S.K.; Hwang, S.-H.; Chang, D.; Kim, S. Preparation of mesoporous In_2O_3 nanofibers by electrospinning and their application as a CO gas sensor. *Sens. Actuators B Chem.* **2010**, *149*, 28–33. [CrossRef]
90. Liu, L.; Zhang, Y.; Wang, G.; Li, S.; Wang, L.; Han, Y.; Jiang, X.; Wei, A. High toluene sensing properties of NiO–SnO_2 composite nanofiber sensors operating at 330 °C. *Sens. Actuators B Chem.* **2011**, *160*, 448–454. [CrossRef]
91. Im, D.; Kim, D.; Jeong, D.; Park, W.I.; Chun, M.; Park, J.-S.; Kim, H.; Jung, H. Improved formaldehyde gas sensing properties of well-controlled Au nanoparticle-decorated In_2O_3 nanofibers integrated on low power MEMS platform. *J. Mater. Sci. Technol.* **2020**, *38*, 56–63. [CrossRef]
92. Lin, Y.; Wei, W.; Li, Y.; Li, F.; Zhou, J.; Sun, D.; Chen, Y.; Ruan, S. Preparation of Pd nanoparticle-decorated hollow SnO_2 nanofibers and their enhanced formaldehyde sensing properties. *J. Alloys Compd.* **2015**, *651*, 690–698. [CrossRef]
93. Gao, X.; Li, F.; Wang, R.; Zhang, T. A formaldehyde sensor: Significant role of pn heterojunction in gas-sensitive core-shell nanofibers. *Sens. Actuators B Chem.* **2018**, *258*, 1230–1241. [CrossRef]
94. Majhi, S.M.; Mirzaei, A.; Kim, H.W.; Kim, S.S. Reduced graphene oxide (rGO)-loaded metal-oxide nanofiber gas sensors: An overview. *Sensors* **2021**, *21*, 1352. [CrossRef]

95. Cho, I.; Kang, K.; Yang, D.; Yun, J.; Park, I. Localized liquid-phase synthesis of porous SnO_2 nanotubes on MEMS platform for low-power, high performance gas sensors. *ACS Appl. Mater. Interfaces* **2017**, *9*, 27111–27119. [CrossRef]
96. Jankiewicz, B.J.; Jamiola, D.; Choma, J.; Jaroniec, M. Silica–metal core–shell nanostructures. *Adv. Colloid Interface Sci.* **2012**, *170*, 28–47. [CrossRef]
97. Lee, J.-H. Gas sensors using hierarchical and hollow oxide nanostructures: Overview. *Sens. Actuators B Chem.* **2009**, *140*, 319–336. [CrossRef]
98. Choi, H.-J.; Kwon, S.-H.; Lee, W.-S.; Im, K.-G.; Kim, T.-H.; Noh, B.-R.; Park, S.; Oh, S.; Kim, K.-K. Ultraviolet photoactivated room temperature NO_2 gas sensor of ZnO hemitubes and nanotubes covered with TiO_2 nanoparticles. *Nanomaterials* **2020**, *10*, 462. [CrossRef]
99. Hazra, A.; Bhowmik, B.; Dutta, K.; Chattopadhyay, P.P.; Bhattacharyya, P. Stoichiometry, length, and wall thickness optimization of TiO_2 nanotube array for efficient alcohol sensing. *ACS Appl. Mater. Interfaces* **2015**, *7*, 9336–9348. [CrossRef]
100. Liu, F.-T.; Gao, S.-F.; Pei, S.-K.; Tseng, S.-C.; Liu, C.-H.J. ZnO nanorod gas sensor for NO_2 detection. *J. Taiwan Inst. Chem. Eng.* **2009**, *40*, 528–532. [CrossRef]
101. Rai, P.; Song, H.-M.; Kim, Y.-S.; Song, M.-K.; Oh, P.-R.; Yoon, J.-M.; Yu, Y.-T. Microwave assisted hydrothermal synthesis of single crystalline ZnO nanorods for gas sensor application. *Mater. Lett.* **2012**, *68*, 90–93. [CrossRef]
102. Wei, Y.; Hu, M.; Yan, W.; Wang, D.; Yuan, L.; Qin, Y. Hydrothermal synthesis porous silicon/tungsten oxide nanorods composites and their gas-sensing properties to NO_2 at room temperature. *Appl. Surf. Sci.* **2015**, *353*, 79–86. [CrossRef]
103. Da Silva, L.F.; Catto, A.C.; Avansi, W., Jr.; Cavalcante, L.S.; Mastelaro, V.R.; Andres, J.; Aguir, K.; Longo, E. Acetone gas sensor based on α-Ag_2WO_4 nanorods obtained via a microwave-assisted hydrothermal route. *J. Alloys Compd.* **2016**, *683*, 186–190. [CrossRef]
104. Zhang, H.; Feng, J.; Wang, J.; Zhang, M. Preparation of ZnO nanorods through wet chemical method. *Mater. Lett.* **2007**, *61*, 5202–5205. [CrossRef]
105. Liu, Y.; Liu, M. Ordered ZnO nanorods synthesized by combustion chemical vapor deposition. *J. Nanosci. Nanotechnol.* **2007**, *7*, 4529–4533. [CrossRef]
106. Chien, F.S.-S.; Wang, C.-R.; Chan, Y.-L.; Lin, H.-L.; Chen, M.-H.; Wu, R.-J. Fast-response ozone sensor with ZnO nanorods grown by chemical vapor deposition. *Sens. Actuators B Chem.* **2010**, *144*, 120–125. [CrossRef]
107. Cha, H.G.; Kim, C.W.; Kim, Y.H.; Jung, M.H.; Ji, E.S.; Das, B.K.; Kim, J.C.; Kang, Y.S. Preparation and characterization of α-Fe_2O_3 nanorod-thin film by metal–organic chemical vapor deposition. *Thin Solid Film.* **2009**, *517*, 1853–1856. [CrossRef]
108. Pradhan, S.K.; Reucroft, P.J.; Yang, F.; Dozier, A. Growth of TiO_2 nanorods by metalorganic chemical vapor deposition. *J. Cryst. Growth* **2003**, *256*, 83–88. [CrossRef]
109. Liu, B.; Hu, Z.; Che, Y.; Allenic, A.; Sun, K.; Pan, X. Growth of ZnO nanoparticles and nanorods with ultrafast pulsed laser deposition. *Appl. Phys. A* **2008**, *93*, 813–818. [CrossRef]
110. Yang, T.; Yu, H.; Xiao, B.; Li, Z.; Zhang, M. Enhanced 1-butylamine gas sensing characteristics of flower-like V_2O_5 hierarchical architectures. *J. Alloys Compd.* **2017**, *699*, 921–927. [CrossRef]
111. Sik, C.M.; Young, K.M.; Mirzaei, A.; Kim, H.-S.; Kim, S.-I.; Baek, S.-H.; Won, C.D.; Jin, C.; Hyoung, L.K. Selective, sensitive, and stable NO_2 gas sensor based on porous ZnO nanosheets. *Appl. Surf. Sci.* **2021**, *568*, 150910.
112. Kim, J.-H.; Mirzaei, A.; Kim, J.-Y.; Yang, D.-H.; Kim, S.S.; Kim, H.W. Selective CO gas sensing by Au-decorated WS_2-SnO_2 core-shell nanosheets on flexible substrates in self-heating mode. *Sens. Actuators B Chem.* **2022**, *353*, 131197. [CrossRef]
113. Xia, Y.; Wang, J.; Chen, R.; Zhou, D.; Xiang, L. A review on the fabrication of hierarchical ZnO nanostructures for photocatalysis application. *Crystals* **2016**, *6*, 148. [CrossRef]
114. Liu, J.; Zhang, L.; Fan, J.; Zhu, B.; Yu, J. Triethylamine gas sensor based on Pt-functionalized hierarchical ZnO microspheres. *Sens. Actuators B-Chem.* **2021**, *331*, 129425. [CrossRef]
115. Cheng, P.; Dang, F.; Wang, Y.; Gao, J.; Xu, L.; Wang, C.; Lv, L.; Li, X.; Zhang, B.; Liu, B. Gas sensor towards n-butanol at low temperature detection: Hierarchical flower-like Ni-doped Co_3O_4 based on solvent-dependent synthesis. *Sens. Actuators B-Chem.* **2021**, *328*, 129028. [CrossRef]
116. Guo, M.; Luo, N.; Chen, Y.; Fan, Y.; Wang, X.; Xu, J. Fast-response MEMS xylene gas sensor based on CuO/WO_3 hierarchical structure. *J. Hazard. Mater.* **2022**, *429*, 127471. [CrossRef]
117. Yu, H.; Guo, C.; Zhang, X.; Xu, Y.; Cheng, X.; Gao, S.; Huo, L. Recent Development of Hierarchical Metal Oxides Based Gas Sensors: From Gas Sensing Performance to Applications. *Adv. Sustain. Syst.* **2022**, *6*, 2100370. [CrossRef]
118. Mirzaei, A.; Janghorban, K.; Hashemi, B.; Neri, G. Metal-core@metal oxide-shell nanomaterials for gas-sensing applications: A review. *J. Nanoparticle Res.* **2015**, *17*, 371. [CrossRef]
119. Yamazoe, N. New approaches for improving semiconductor gas sensors. *Sens. Actuators B Chem.* **1991**, *5*, 7–19. [CrossRef]
120. Mirzaei, A.; Yousefi, H.R.; Falsafi, F.; Bonyani, M.; Lee, J.-H.; Kim, J.-H.; Kim, H.W.; Kim, S.S. An overview on how Pd on resistive-based nanomaterial gas sensors can enhance response toward hydrogen gas. *Int. J. Hydrogen Energy* **2019**, *44*, 20552–20571. [CrossRef]
121. Iordache, S.M.; Ionete, E.I.; Iordache, A.M.; Tanasa, E.; Stamatin, I.; Grigorescu, C.E.A. Pd-decorated CNT as sensitive material for applications in hydrogen isotopes sensing-Application as gas sensor. *Int. J. Hydrogen Energy* **2021**, *46*, 11015–11024. [CrossRef]
122. Li, G.; Fan, Y.; Hu, Q.; Zhang, D.; Ma, Z.; Cheng, Z.; Wang, X.; Xu, J. Morphology and size effect of Pd nanocrystals on formaldehyde and hydrogen sensing performance of SnO_2 based gas sensor. *J. Alloys Compd.* **2022**, *906*, 163765. [CrossRef]

123. Shen, S.-K.; Cui, X.-L.; Guo, C.-Y.; Dong, X.; Zhang, X.-F.; Cheng, X.-L.; Huo, L.-H.; Xu, Y.-M. Sensing mechanism of Ag/α-MoO_3 nanobelts for H_2S gas sensor. *Rare Met.* **2021**, *40*, 1545–1553. [CrossRef]
124. Kim, J.-H.; Kim, S.S. Realization of ppb-scale toluene-sensing abilities with Pt-functionalized SnO_2–ZnO core–shell nanowires. *ACS Appl. Mater. Interfaces* **2015**, *7*, 17199–17208. [CrossRef]
125. Kim, J.-H.; Wu, P.; Kim, H.W.; Kim, S.S. Highly selective sensing of CO, C6H6, and C_7H_8 gases by catalytic functionalization with metal nanoparticles. *ACS Appl. Mater. Interfaces* **2016**, *8*, 7173–7183. [CrossRef]
126. Li, X.; Yu, J.; Wageh, S.; Al-Ghamdi, A.A.; Xie, J. Graphene in photocatalysis: A review. *Small* **2016**, *12*, 6640–6696. [CrossRef]
127. Schedin, F.; Geim, A.K.; Morozov, S.V.; Hill, E.W.; Blake, P.; Katsnelson, M.I.; Novoselov, K.S. Detection of individual gas molecules adsorbed on graphene. *Nat. Mater.* **2007**, *6*, 652–655. [CrossRef]
128. Chatterjee, S.G.; Chatterjee, S.; Ray, A.K.; Chakraborty, A.K. Graphene–metal oxide nanohybrids for toxic gas sensor: A review. *Sens. Actuators B Chem.* **2015**, *221*, 1170–1181. [CrossRef]
129. Pendolino, F.; Armata, N. *Graphene Oxide in Environmental Remediation Process*; Springer: Berlin/Heidelberg, Germany, 2017; Volume 11.
130. Hummers, W.S., Jr.; Offeman, R.E. Preparation of graphitic oxide. *J. Am. Chem. Soc.* **1958**, *80*, 1339. [CrossRef]
131. Brodie, B.C. Hydration behavior and dynamics of water molecules in graphite oxide. *Ann. Chim Phys.* **1860**, *59*, 466–472.
132. Shewale, P.S.; Yun, K.-S. Synthesis and characterization of Cu-doped ZnO/RGO nanocomposites for room-temperature H_2S gas sensor. *J. Alloys Compd.* **2020**, *837*, 155527. [CrossRef]
133. Liu, Z.; Yu, L.; Guo, F.; Liu, S.; Qi, L.; Shan, M.; Fan, X. Facial development of high performance room temperature NO_2 gas sensors based on ZnO nanowalls decorated rGO nanosheets. *Appl. Surf. Sci.* **2017**, *423*, 721–727. [CrossRef]
134. Jia, A.; Liu, B.; Liu, H.; Li, Q.; Yun, Y. Interface design of SnO_2@PANI nanotube with enhanced sensing performance for ammonia detection at room temperature. *Front. Chem.* **2020**, *8*, 383. [CrossRef]
135. Amiri, V.; Roshan, H.; Mirzaei, A.; Neri, G.; Ayesh, A.I. Nanostructured metal oxide-based acetone gas sensors: A review. *Sensors* **2020**, *20*, 3096. [CrossRef]
136. Sharma, H.J.; Salorkar, M.A.; Kondawar, S.B. H_2 and CO gas sensor from SnO_2/polyaniline composite nanofibers fabricated by electrospinning. *Adv. Mater. Proc.* **2017**, *2*, 61–66. [CrossRef]